ARMY RESEARCH LABORATORY

Responses of a Water Barricade and an Acceptor Stack to the Detonation of a Donor Munitions Stack

Richard E. Lottero

ARL-TR-1600 MARCH 1998

The findings in this report are not to be construed as an official Department of the Army position unless so designated by other authorized documents.

Citation of manufacturer's or trade names does not constitute an official endorsement or approval of the use thereof.

Destroy this report when it is no longer needed. Do not return it to the originator.

Army Research Laboratory
Aberdeen Proving Ground, MD 21005-5066

ARL-TR-1600 March 1998

Responses of a Water Barricade and an Acceptor Stack to the Detonation of a Donor Munitions Stack

Richard E. Lottero
Weapons & Materials Research Directorate

Abstract

This report documents the numerical modeling of the detonation of a simplified munitions stack, referred to as the "donor" stack, in a temporary storage area and the subsequent effects on the immediate surroundings of the stack. A plausible configuration of a donor munitions stack, a water barricade, and an "acceptor" munitions stack is modeled in a two-dimensional (2-D) Cartesian hydrocode computation using the CTH hydrodynamics computer code. The donor stack is modeled as an uncased condensed high-explosive charge with a rectangular cross section. The water barricade has a trapezoidal cross section, and the acceptor stack is a solid rectangle. The loading on and pressures within the barricade are computed, as is the whole-body motion of the barricade. A separate computation was then run with the water barricade, reconstituted into its original shape and translating at the late-time velocity from the first computation, interacting with the acceptor stack. These computations were performed as part of a U.S. Army Research Laboratory (ARL) study entitled "Munitions Survivability Technology," sponsored by the U.S. Army Defense Ammunition Logistics (Ammolog) Activity.

ACKNOWLEDGMENTS

The technical consultation of Drs. Robert Frey and John Starkenberg of ARL and the technical support from Robert Rossi and Duane Scarborough of the U.S. Army Defense Ammunition Logistics Activity are gratefully acknowledged.

INTENTIONALLY LEFT BLANK

TABLE OF CONTENTS

INTENTIONALLY LEFT BLANK

LIST OF FIGURES

LIST OF FIGURES (continued)

LIST OF FIGURES (continued)

INTENTIONALLY LEFT BLANK

1. INTRODUCTION

When military units are involved in rapid deployment or rapid movement situations, it is not always possible to store needed munitions using standard safe-distance guidelines. At times such as these, it is sometimes considered necessary by commanders in the field to store munitions in closely spaced stacks in the open with no protective barricades between them. The primary purpose of protective barricades is to prevent a direct, line-of-sight path for either blast or fragments from existing between munitions stacks in proximity to one another. One example of extremely close spacing of munitions stacks occurred in the buildup of ammunition stocks at the port of Al Jubayl, Saudia Arabia, before the opening of hostilities in the Gulf War. A photograph of the port is shown in Figure 1. At one

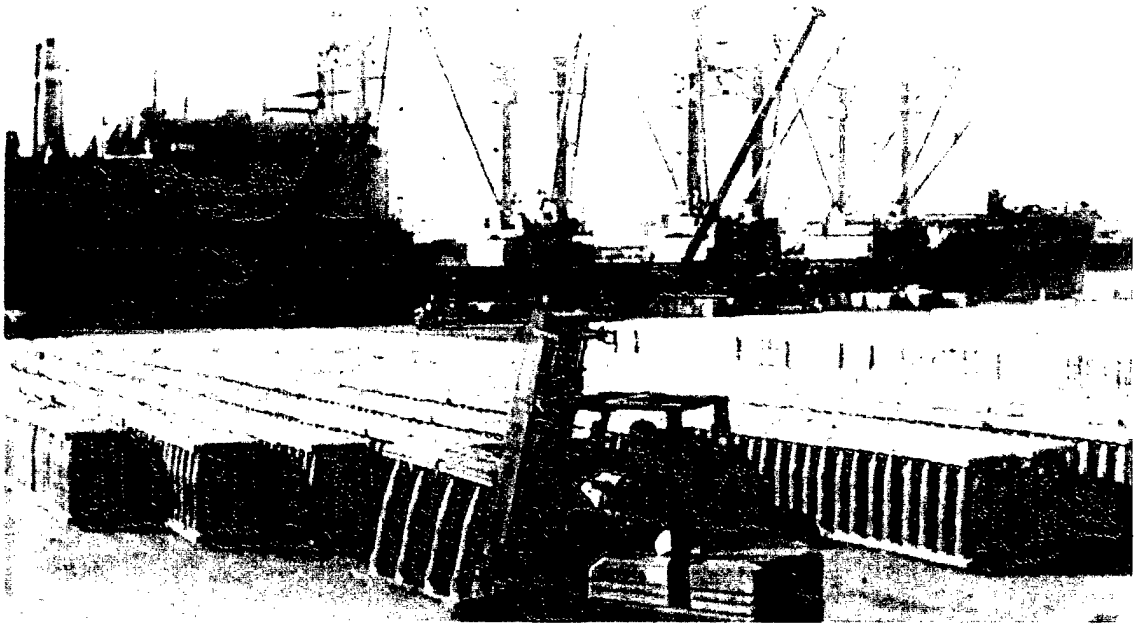

Figure 1. Munitions Being Off-Loaded at Al Jubayl, Saudia Arabia, 1991 (courtesy of D. Scarborough, U.S. Army Defense Ammunition Logistics Activity).

point, the stocks were estimated to have a net explosive weight (NEW) of 30,000 short tons. This stockpile, along with much of the port itself, could have been destroyed with one direct hit or other initiating incident. Fortunately, none occurred. Later, there was a similar situation involving munition stockpiles after the end of hostilities at Doha, Kuwait, in 1991. The munitions storage area also included nearby military vehicles, many of which contained combat loads. A fire in one vehicle started a chain reaction, which resulted in the loss of a large amount of munitions and equipment. Figure 2 shows a photograph taken at Doha during the actual event, in which large, unidentified pieces of debris may be seen traveling high in the air on ballistic trajectories. The next three figures were taken after the event at Doha had ended but before cleanup operations had begun. Figure 3 shows a section of

Figure 2. Doha, Kuwait, 1991, During the Fire and Explosion Event (courtesy of D. Scarborough, U.S. Army Defense Ammunition Logistics Activity).

the storage area strewn with debris from munitions. Figure 4 shows a close-up of some of the destroyed self-propelled artillery and Figure 5 shows a row of armored vehicles (some damaged) at what appears to be a border of the fire and explosion event.

The U.S. Army Defense Ammunition Logistics (Ammolog) Activity, working within the Department of the Army, has established an Army Science and Technology Objective entitled "Munitions Survivability." Its primary objective is to improve the chances of stopping the chain reaction propagation from stack to stack after a munitions stack has been initiated. Ideally, the goal is to confine the event to just the single, initial munitions stack. The task assigned to the U.S. Army Research Laboratory (ARL), sponsored by Ammolog, is entitled "Munitions Survivability Technology." Its focus is on characterizing the nature of the reaction(s) within a donor stack; the propagation of fragments, firebrands, and blast; the protection provided to potential acceptor stacks by barricades of various designs (provided by others within the program); the effects on the barricades themselves; and the possible or probable reactions by the acceptor stack. This report documents one part of a larger computational study, focusing on the complete, high-order detonation of a postulated donor stack and the subsequent effects on an acceptor stack protected by a candidate water-filled barricade.

Figure 3. Doha, Kuwait, 1991, Destroyed Munitions (courtesy of D. Scarborough, U.S. Army Defense Ammunition Logistics Activity).

Figure 4. Doha, Kuwait, 1991, Destroyed Self-Propelled Artillery (courtesy of D. Scarborough, U.S. Army Defense Ammunition Logistics Activity).

Figure 5. Doha, Kuwait, 1991, Destroyed Munitions With Nearby Armored Vehicles (courtesy of D. Scarborough, U.S. Army Defense Ammunition Logistics Activity).

2. COMPUTATIONAL APPROACH AND GEOMETRY

2.1. General Comments on the Hydrocode Model

The two computations that are reported here were performed using the CTH[1] hydrocode developed at Sandia National Laboratories, Albuquerque, NM. CTH solves the inviscid Euler equations using a second-order accurate, explicit time-stepping method. It has a Lagrangian first phase and a second phase that uses a mesh remapping to bring the distorted mesh back to the stationary Eulerian mesh and thereby perform a second-order accurate fluxing of materials between cells. The conservation equations are replaced by finite-volume approximations to maximize the code's ability to conserve mass, momentum, and energy. The computational grid cells have rectangular cross sections in two-dimensional (2-D) Cartesian coordinates with a presumed unit depth (1.0 cm). This unit depth represents an infinite depth with no wave interactions or fluxing in that direction. The computational grid cells in three-dimensional (3-D) Cartesian coordinates are rectangular parallelepipeds and therefore have rectangular cross sections in any planes parallel to any pair of axes. The computational grid cells in 2-D cylindrical coordinates are toroidal rings with rectangular cross sections. All axes are orthogonal. The reader is referred to the appropriate users' manuals for practical

information about the structure and use of the CTHGEN[2] grid generation code, the CTH[3] hydrocode, and their supporting utilities.

Ideally, a meaningful subsection of a postulated munitions storage area should be modeled in a 3-D Cartesian computational grid. Individual munitions stacks surrounded by barricades would be modeled, with one of the stacks designated as the donor stack. With such a grid design, most of the first-order physics of the system could be modeled. However, at this early stage of the computational study, that level of detail is not warranted. There are no firm definitions yet of the most likely munitions stack dimensions, the specific munitions, and the recommended maximum NEW of the stacks. The barricade geometric design and materials are not yet final, nor are the recommended standoff distances. Hopefully, the successful pursuit of this overall program will produce much of that information.

After much discussion, it was decided that these early computations would be performed using relatively simple physical approximations to provide initial estimates of simple blast loads and responses. These estimates could then be used as input to increasingly refined computational and experimental efforts. The first decision was to model the donor stack in the first computation discussed herein, designated as Computation 970908, as an uncased charge with no packing materials. This reduced the analysis to one of blast loading only, with no production of fragments or other debris. The second decision was to represent the explosive mass in Computation 970908 as a single, condensed charge rather than as a distributed set of smaller condensed charges. Preliminary computations with a single condensed charge versus distributed condensed charges of the same total mass showed comparable loading on and response of a simple barricade shape. More detailed comparisons of different configurations may be made later in another part of this study. The third decision was to model the flow field in 2-D Cartesian coordinates for this computation and for the second discussed herein, which is designated as Computation 971001. This provided a worst case blast loading for the simplified, uncased charge of condensed high explosives by eliminating the possibility of having any compression or expansion waves in the direction of depth of the munitions stacks and barricade. (Depth is a measure parallel to both the ground and the side walls of the munitions stack.) In effect, the donor and acceptor stacks and the barricade have an infinite depth in that coordinate system. In the CTH hydrocode model, which uses the cgs (centimeter-gram-second) units system, this implies a unit depth of 1.0 cm.

2.2. The Donor Munitions Stack

A previous ARL report on fragment propagation probabilities by Starkenberg et al.,[4] used palletized and single M107 155-mm projectiles as fragment donors to analyze the threat to palletized TOW-2A missiles as acceptor munitions. That report was used as a guide from which to select the dimensions of a representative munitions stack. The donor munitions stack for the current study was assumed be of the same size as one consisting of 72 pallets of M107 155-mm projectiles, stacked three pallets high by four wide by six deep. Each pallet

contains eight rounds. The dimensions of this particular stack are 2.44 m high by 2.94 m wide by 2.19 m deep (8.00 ft by 9.63 ft by 7.20 ft). Other stacking configurations and dimensions for the same number of pallets of M107 munitions are also possible but are not discussed here. According to Starkenberg et al.,[4] "Storage regulations applicable to basic load ammunition holding areas in theaters of operations limit the explosive quantity in any stack to 4,000 kg.... (See Army Regulation 385-64.)" A single M107 round can contain either 6.62 kg (14.6 lbm, where "lbm" denotes pounds mass, avoirdupois) of TNT or 6.98 kg (15.4 lbm) of Comp-B. A pallet contains eight rounds. The total mass of a pallet, including packaging, is 362 kg (797 lbm).[5] Thus, a presumed stack of M107 munitions would contain 576 rounds, having a total mass of 4,024 kg (8,870 lbm) of Comp-B. For simplicity, the nominal explosive mass of Comp-B for this computational study was taken as 4,000 kg (8,818 lbm) of Comp-B for the donor stack. The total mass of an actual stack containing 72 pallets of M107 rounds is 26,029 kg (57,384 lbm), including all packaging materials. This equates to a mass of 118.61 kg/cm depth for the actual stack with all materials. The acceptor stack was assumed to be of the same physical dimensions and total mass as those of the donor stack.

As stated previously, it was decided to model the donor stack in Computation 970908 as an uncased explosive charge. The explosive modeled was Comp-B, taken at its reference density of 1.72 g/cm^3 in its undetonated state, and modeled[6] within the Sesame[7] equation-of-state package. The Sandia National Laboratories' Sesame equation-of-state package includes tabular data for high explosives and separate implementations of data for the Mie-Gruneisen, Jones-Wilkins-Lee (JWL), and ideal-gas equations of state. The explosive charge was placed within the computational flow field with its center coincident with that of the M107 donor stack described before. After assigning the donor stack the nominal explosive mass of 4,000 kg and using the actual stack depth of 2.19 m, this equated to an explosive charge mass of approximately 18.227 kg/cm depth of the stack to be modeled in the unit-depth 2-D Cartesian coordinates flow field in CTH. This mass of Comp-B was modeled as a rectangle whose width and height are in direct proportion to those for the donor stack. Specifically, the explosive charge is 93.91 cm high and 113.04 cm wide (i.e., the full width, and not one-half width for symmetry), located with its center of mass 121.92 cm above the ground plane. The ground plane was designated as a perfectly reflective boundary.

A small central section of the explosive charge served as a computational "booster" charge. It was detonated using the programmed burn[2] model using a constant detonation velocity 7.98 km/s for reference-density Comp-B.[8] This model simulates the complete detonation of any part of an explosive that is passed by the expanding theoretical detonation front moving at that constant velocity. The remainder of the detonation was modeled using the "history variable reaction burn" (HVRB) model.[7] The HVRB model evaluates the thermodynamic state of a mass of undetonated explosive in a given computational flow field cells to determine if that material should be detonated in that time step. The detonation initiation point was located at the center of the explosive charge at the (X,Y) point (0.0,121.92 cm).

2.3. The Barricade

The barricade shape chosen for Computations 970908 and 971001 is similar to that proposed by a Small Business Innovative Research (SBIR) contractor.[9] That design consists of a pyramidal stacking of a number of identical, cylindrical, water-filled tubes. For simplicity in these computations, it is assumed that the stacking results in a shape that has a continuous sloping side with an inside angle, θ, at the top that is equal to 30 degrees when measured from a line perpendicular to the ground plane. An idealized trapezoidal cross section that has no internal air spaces and consists only of water is assumed. The materials that comprise the tubes' walls are ignored. The height of the barricade, H, is 243.84 cm (8.0 ft) as stated in the contract. The width of the barricade at the flat top, W_t, is assumed for the purposes of this computational study as 1.0 m (3.28 ft). The width of the barricade at the base, W_b, is then $W_b = W_t + 2H\tan(\theta)$, or 381.56 cm (12.52 ft) for this geometry. The mass of water for the barricade is 58.71 kg/cm depth. The water in the barricade was modeled using the CTH Sesame equation-of-state data for water.[10] The bottom corner of the barricade closest to the donor stack was placed at a standoff distance of 3.048 m (10 ft) from nearest side of the donor stack. The standoff distance here is measured from the face of what would have been the side of the munitions stack, not the condensed explosive charge representing the stack.

2.4. The Acceptor Munitions Stack

The acceptor munitions stack was modeled in Computation 970908 as a simple, relatively inert mass of iron[11] with the same height and width (2.44 m high by 2.94 m wide) as the reference M107 munitions stack. The acceptor stack was located at a standoff distance of 3.048 m between its nearest face and the bottom corner of the barricade farthest from the donor stack. The purpose in modeling the acceptor stack in Computation 970908 as a full-sized mass of iron was for the convenience of having an object with the correct physical dimensions in order to observe wave interactions on the surface and providing surface blast loading data through the use of CTH's massless "tracer" particles placed in the air near the surfaces. Tracer particles are massless points that are specified at desired locations by the user at grid generation time. They may be fixed in computational space or be free to move along one or more of the principal axes in the grid. A relatively full complement of data describing the thermodynamic state and other physical parameters at the location of each tracer is recorded for later processing by the user. The use of iron was a simple convenience to provide a massive, relatively non-responding object. The acceptor stack was also modeled as iron in Computation 971001, with the height being the same but having the width adjusted to 61.96 cm so that the mass of the acceptor stack per centimeter depth in the computation was equal to that of the actual M107 stack described previously.

3. THE HYDROCODE COMPUTATIONS

3.1. Donor Stack Detonation and Barricade Loading and Response

The first of the two computations, Computation 970908, was focused on modeling the detonation of the donor stack and the blast loading on the water barricade and acceptor stack; the coupled response of the barricade was computed during this blast loading. Both the whole-body response and the internal dynamics of the barricade were of interest, as was studying how the barricade shape might redirect the blast away from the acceptor stack. The second computation, numbered 971001, then used the barricade, reconstituted into its original shape and traveling toward the acceptor stack at its final X-direction velocity from Computation 970908, as an impactor striking the acceptor stack. Figure 6 shows the computational flow field at the start of Computation 970908 at the instant of the initiation of the detonation at time equal to zero. The "Y" axis at the left of the figure represents the height measured from the ground plane. In this simple 2-D Cartesian coordinate system, the left boundary at the Y axis is designated as a perfectly reflective plane of symmetry. The "X" axis represents the measure of width in the system and coincides with the perfectly reflective ground plane. The Y axis at the X = 0.0 location is also a vertical bisector of the donor stack. The air in the flow field, modeled with data from Graboske[12]within the Sesame[7] equation-of-state package, is shown with the color yellow. The top and right transmissive boundaries are marked by the top and right edges of that yellow region. The explosive charge representing the donor stack is shown as the red (one-half) rectangle on the left symmetry boundary, the water barricade is shown as the blue trapezoid, and the acceptor stack is shown as the black rectangle (the object closest to the right transmissive boundary).

Figure 7 shows the computational flow field at 0.25 ms after the initiation of the detonation (hereinafter referred to as "initiation") of the donor stack. The detonation process had already been completed by this time (theoretically at 0.092 ms). The expanding explosive products and leading shock are just now interacting with the bottom transmissive boundary and have not yet reached the X = 2.0 m point.

Figure 8 shows the computational flow field at 0.75 ms after initiation. The leading edge of the air shock moving outward along the bottom boundary has just begun its interaction with the bottom corner of the barricade. The leading edge of the explosive products is following just behind the air shock and is located at approximately X = 4.0 m. A shock that has reflected from the bottom boundary is also now moving upward through the explosive products. The shock contours are represented by a "white-out" of the colors for the various materials. The actual values associated with the shock contours are not critical to understanding the results at this point. The primary purpose of including these figures with the shock contours and the material maps is to provide a qualitative impression of the dynamics of the interaction process. Quantitative data will follow later.

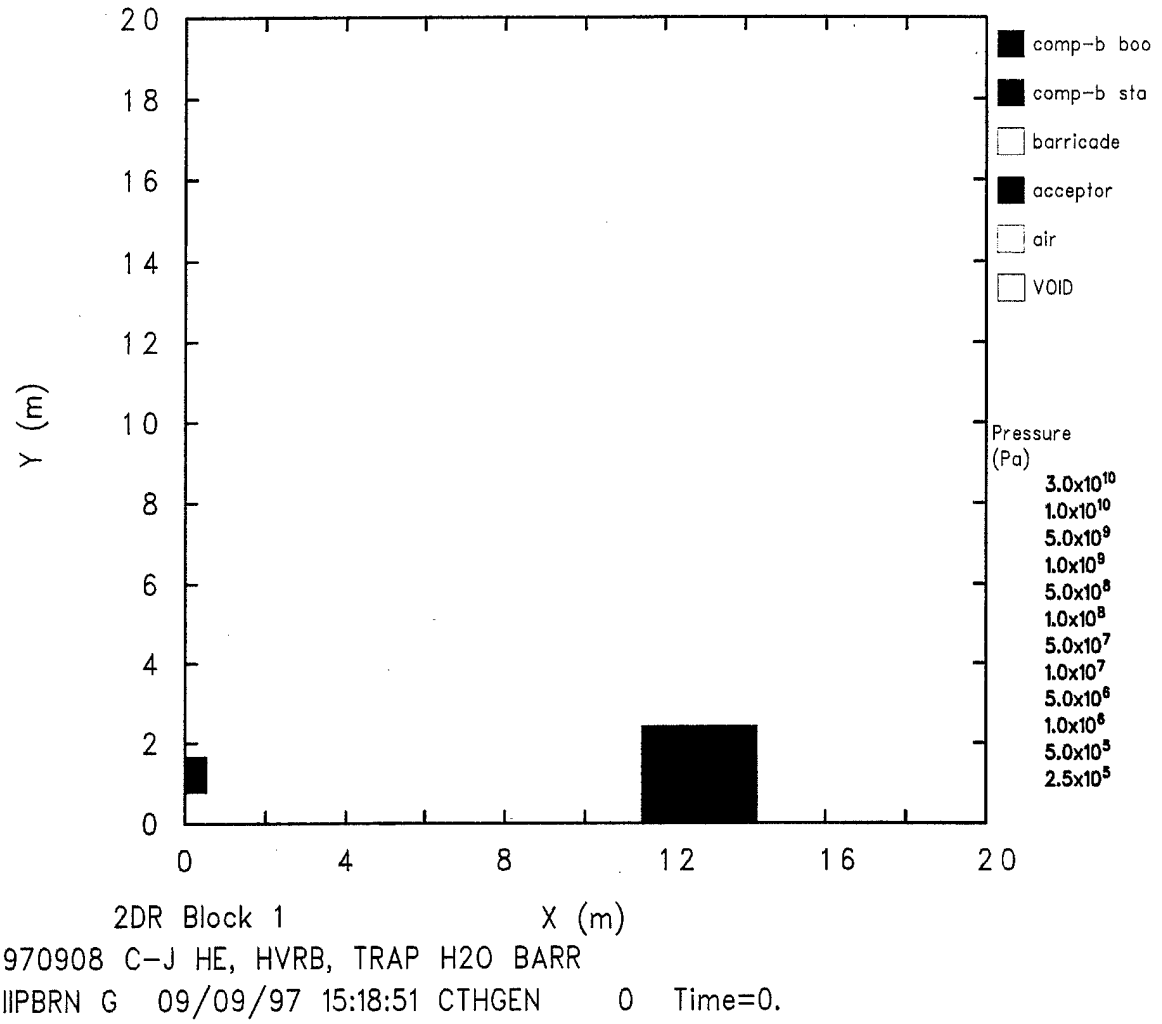

Figure 6. Flow Field at Time = 0.0 for Computation 970908.

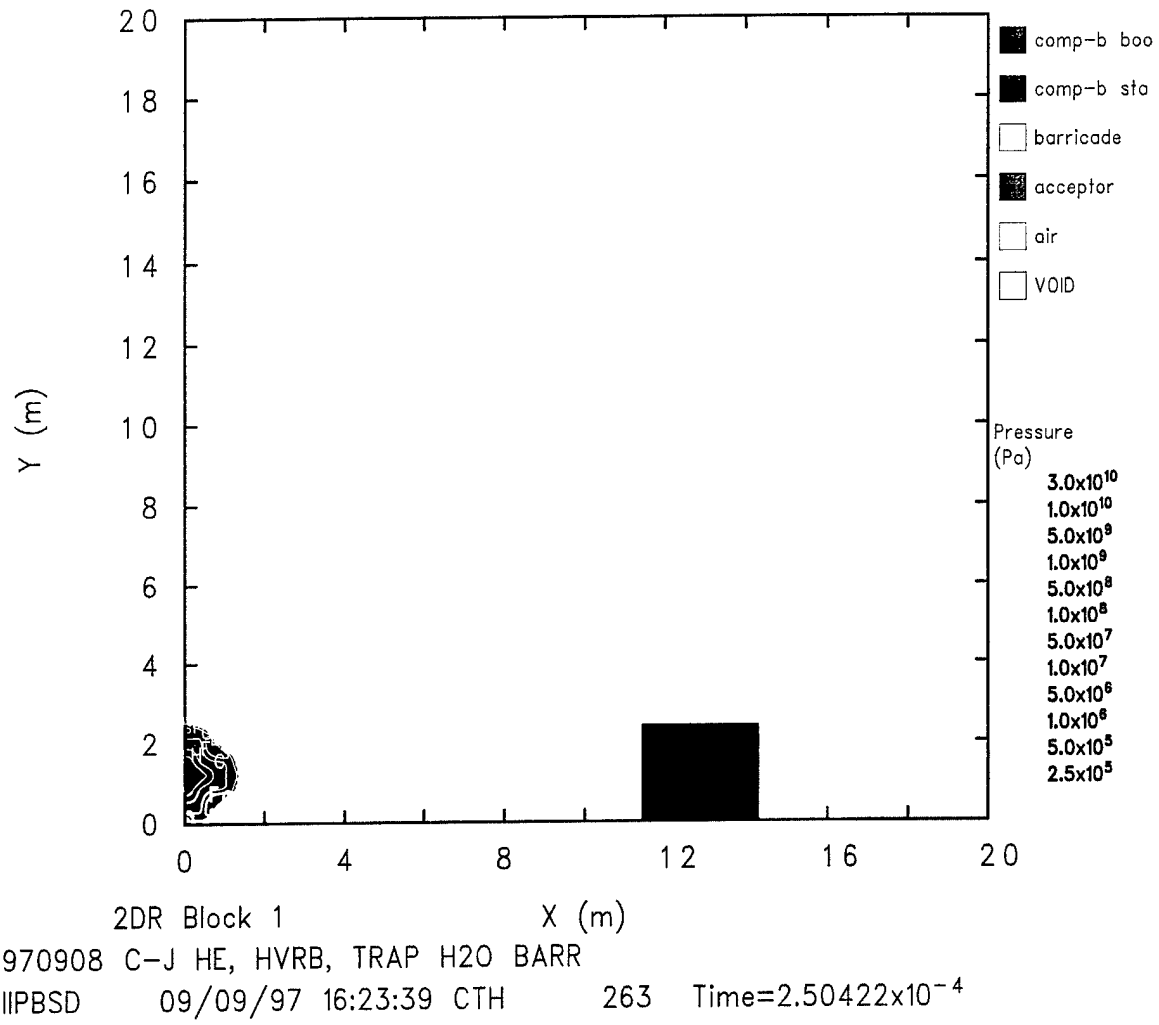

Figure 7. Flow Field at Time = 0.25 ms for Computation 970908.

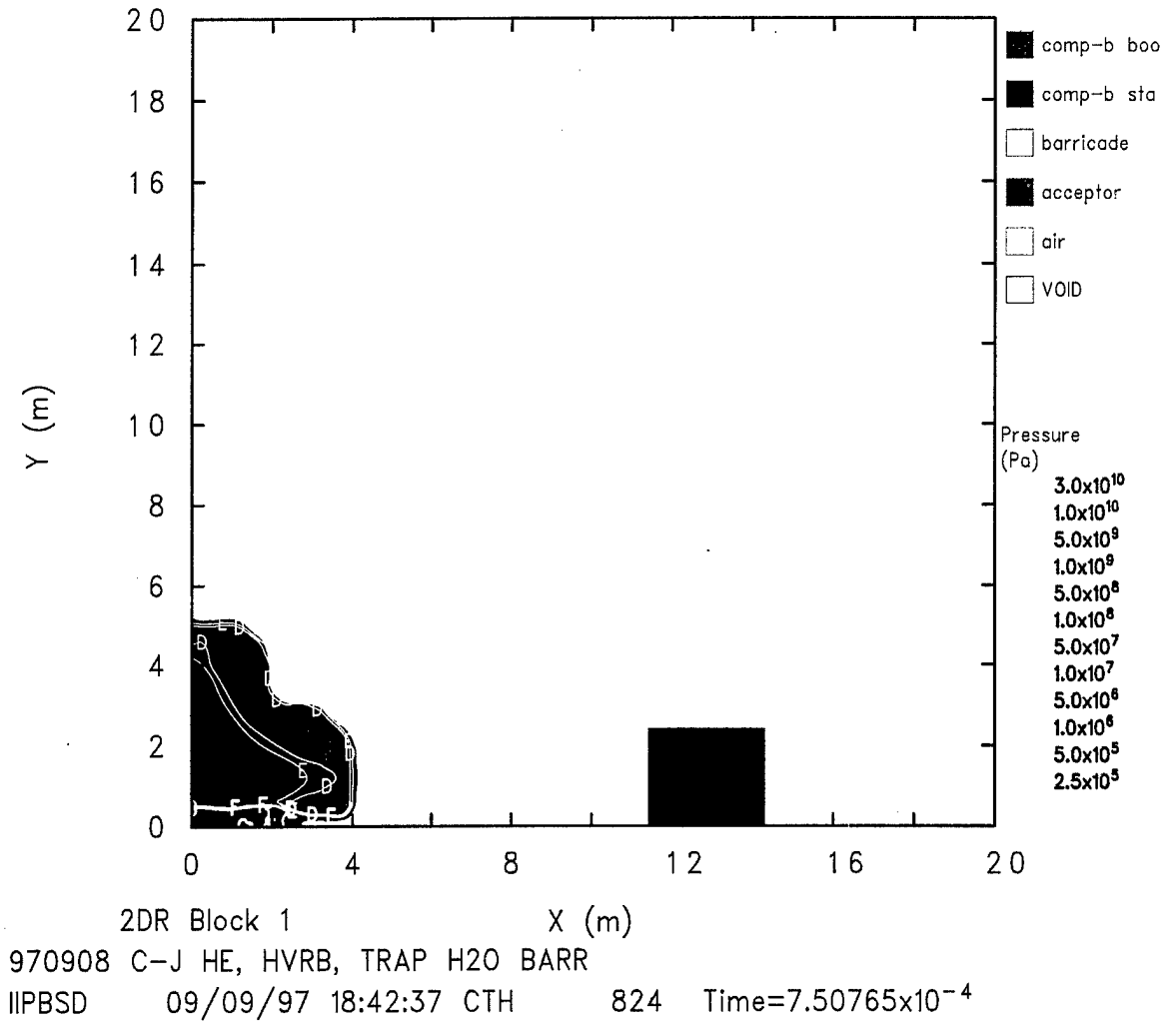

Figure 8. Flow Field at Time = 0.75 ms for Computation 970908.

Figure 9 shows the computational flow field at 2.50 ms after initiation. The leading air shock and the explosive products have now interacted with the entire left surface of the barricade, which is beginning to show distortion and some translation toward the acceptor stack. However, the transfer of momentum and energy from the air shock and the explosive products has not yet been completed. The shock in the water has just reached the bottom-right corner of the barricade, and the spall-like acceleration of the sloping right surface of the barricade is under way. The combined interactions of the explosive products with the reflective ground plane and the barricade have caused much of the explosive products to be directed upward and away from the acceptor stack. The leading air shock, strongly curved and relatively weak because of the expansion over and around the barricade, is now just under 1.5 m from interacting with the top left corner of the acceptor stack.

Figure 10 shows the computational flow field at 5.00 ms after initiation. The barricade is now significantly distorted and traveling at close to its maximum velocity in the X direction. The air shock has almost fully engulfed the acceptor stack. The explosive products and associated air blast are continuing to be directed primarily upward and away from the acceptor stack. The computation was stopped at 8.0 ms, at which time the barricade had essentially reached a steady final velocity, the determination of which was the primary goal of Computation 970908.

One of the several useful features of the CTH hydrocode is its ability to extract the bulk momentum along a given axis for a material. From that bulk momentum, many useful parameters can be derived to describe the motion of and forces on an object comprised of a uniquely defined material. The barricade constitutes the only water in the computational flow field, and its motion in the X direction toward the acceptor stack is of interest here. Figure 11 shows the bulk momentum of the water barricade in the X direction, with positive momentum in the direction of increasing values of X, moving toward the acceptor stack. Hereinafter, any use of the term "momentum" or the other variables derived from it should be construed as referring to the bulk value in the X direction per centimeter depth, unless specifically stated otherwise. The momentum has reached a constant value of 10.18 Mg-m/s by 8.0 ms, the ending time of the computation, implying a steady X-direction velocity. As may be seen in Figure 11, the momentum versus time curve is relatively smooth and well behaved, making it easier to extract other data from it. The X-direction velocity of the water barricade toward the acceptor stack is shown in Figure 12. This was computed by dividing the time-dependent momentum of the barricade by its mass, 58.71 kg/cm depth. The X-direction velocity of the barricade at 8.0 ms was steady at 173.4 m/s. One way to measure the forces on and within the barricade is to determine the acceleration rate of the barricade and view it in terms of multiples of the standard acceleration of gravity at the Earth's surface, designated here by the symbol "G," where G = 9.80665 m/s^2. The velocity shown in Figure 12 was piecewise differentiated with respect to time, using the difference values of velocity and time in the data file. The acceleration data were then divided by the value for G. The acceleration versus time for the barricade is shown in Figure 13, in which the ordinate is labeled "Earth G's" for clarity. The acceleration has a double peak, with the

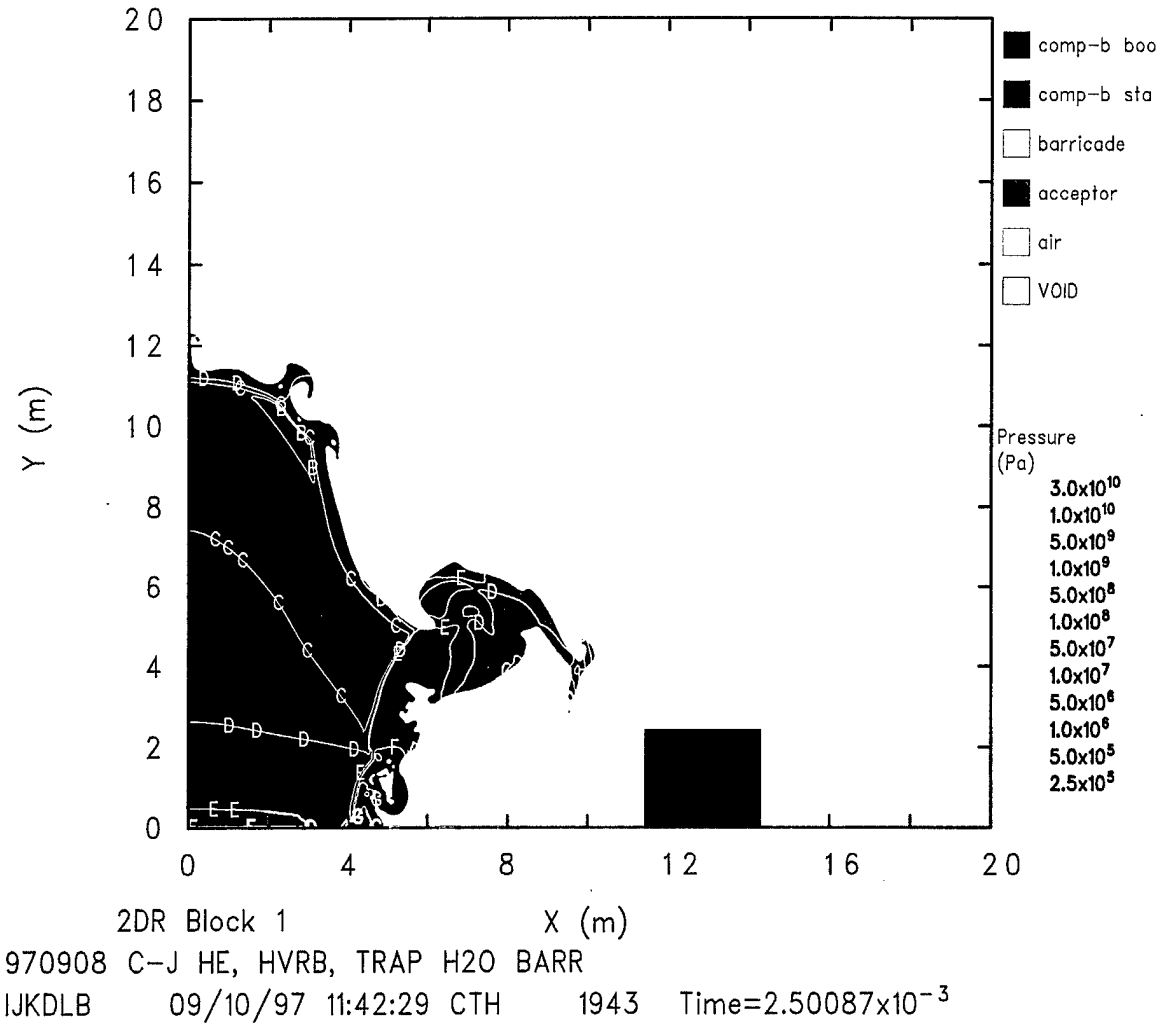

Figure 9. Flow Field at Time = 2.50 ms for Computation 970908.

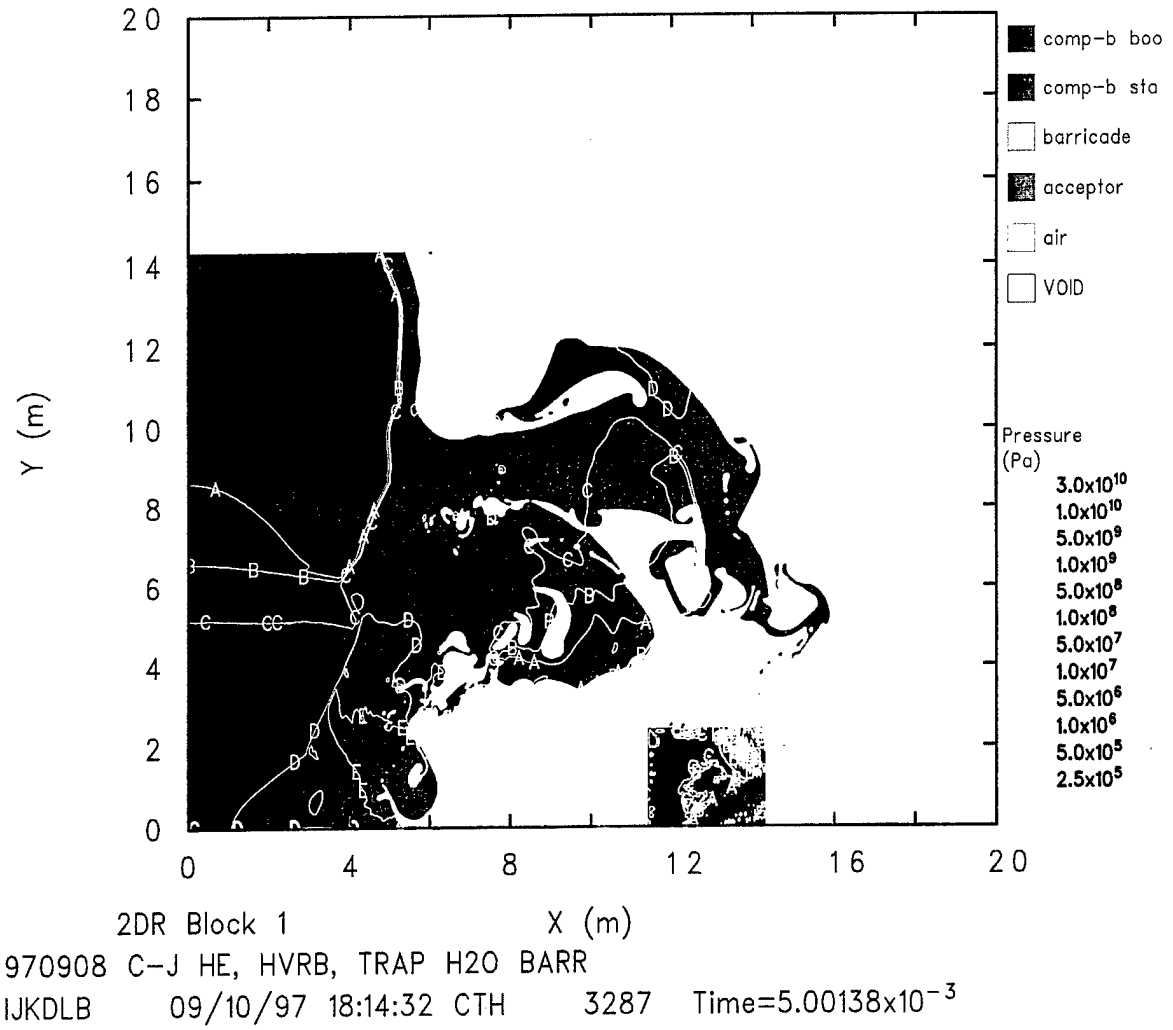

Figure 10. Flow Field at Time = 5.00 ms for Computation 970908.

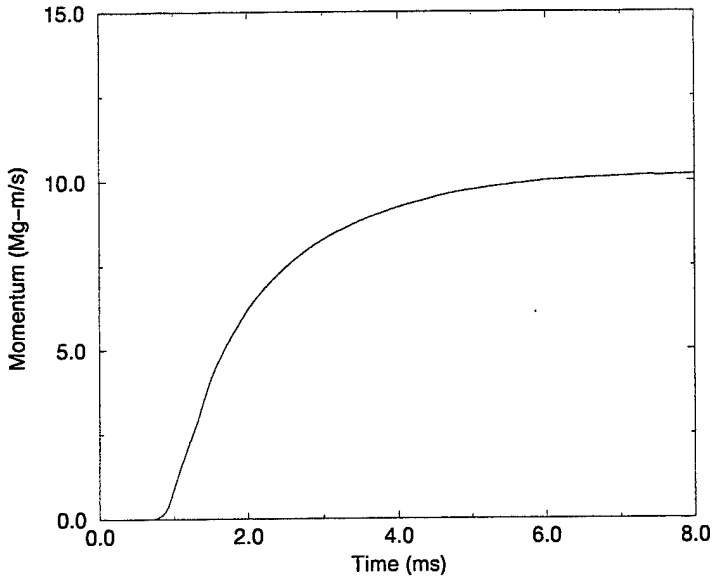

Figure 11. Water Barricade Bulk X-Direction Momentum Toward Acceptor Stack, Computation 970908.

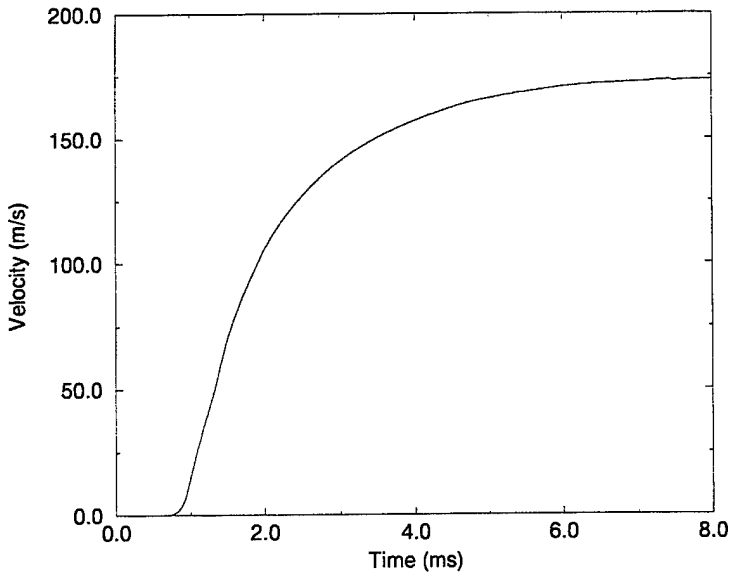

Figure 12. Water Barricade X-Direction Velocity Toward the Acceptor Stack, Computation 970908.

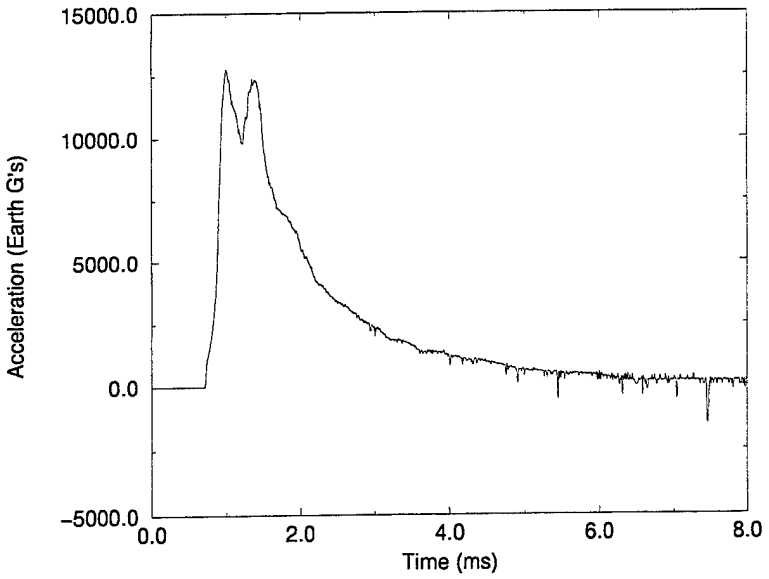

Figure 13. Water Barricade X-Direction Acceleration Toward the Acceptor Stack, Computation 970908.

first and larger peak of 12,770 G's occurring at 1.00 ms, and the second peak of 12,350 G's occurring at 1.38 ms. Finally, the velocity data are used to compute the bulk translation of the barricade versus time, which is shown in Figure 14. By the ending time of 8.0 ms, the barricade has moved 101.8 cm and is traveling at its final, maximum velocity of 173.4 m/s toward the acceptor stack.

In addition to determining the bulk reaction of the water barricade, it is also necessary to study the loading and motion at various locations on and within the barricade. The CTH hydrocode allows the user to distribute tracer particles, described earlier, at locations within the computational grid where detailed data are desired. The first set of tracers that will be discussed was placed just inside the sloping left surface of the barricade that faces the donor stack. Twenty tracers were evenly distributed, from top to bottom, about 1.0 cm below the surface, measured along a line perpendicular to the surface. Figure 15 shows an unweighted average of the overpressure versus time for those 20 tracers. The peak average overpressure of 293.7 MPa (42,600 psi, where "psi" is pounds force per square inch [lbf/inch^2]) occurred at 1.35 ms. These early-time data should be considered reliable because the tracers are still in essentially water-filled computational flow field cells. The later data, probably after 2.0 ms, are not as reliable an indicator of the average overpressure specific to the left surface of the water. This is because of the distortion of the barricade with time; the mixing of air, explosive products, and water; and the freedom given to the tracer particles to move in both the X and Y directions in response to the blast loading. Pressures computed in mixed-material cells are not as reliable or as rigorously determined as are those in single-

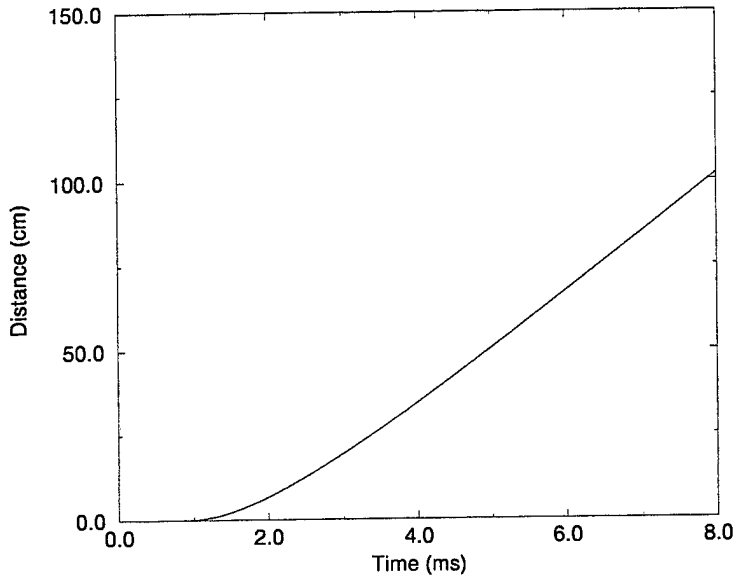

Figure 14. Water Barricade X-Direction Distance Moved Toward the Acceptor Stack, Computation 970908.

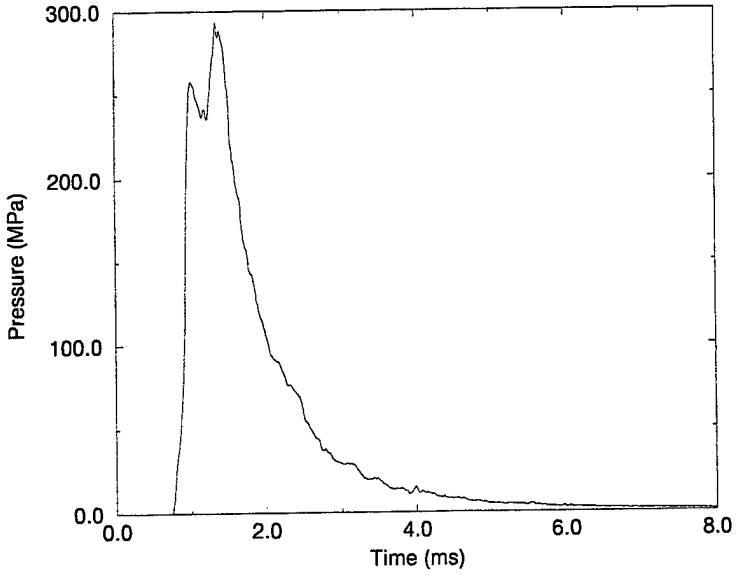

Figure 15. Average Overpressure Inside the Left Surface of the Water Barricade, Computation 970908.

material cells. Also, some of the tracers may no longer be located just under the increasingly distorted left surface of the barricade, and they may have moved enough that the original even spacing assumed for the averaging may no longer exist. Figure 16 shows the average X-

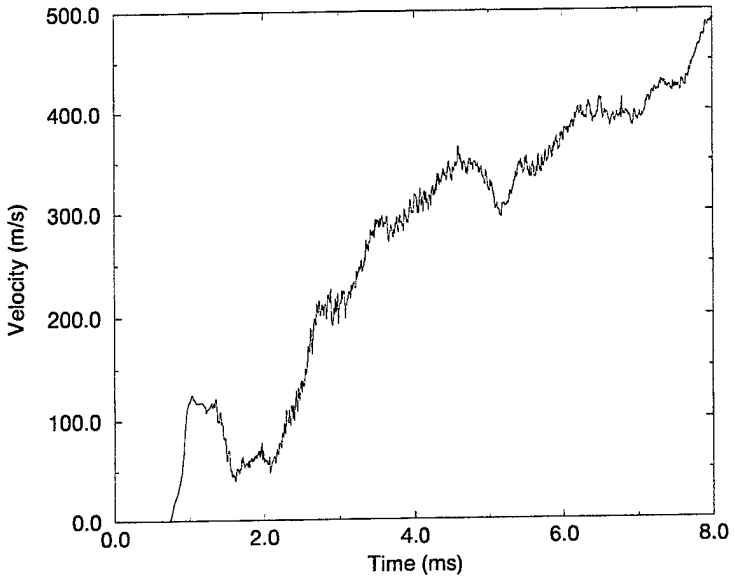

Figure 16. Average X-Direction Velocity Inside the Left Surface of the Water Barricade, Computation 970908.

direction velocity for that same set of tracers. The final X-direction velocity of 490.6 m/s at 8.0 ms for these tracers is nearly three times the final bulk X-direction velocity of 173.4 m/s for the entire mass of water that constitutes the barricade. This indicates that there is also a large Y-direction velocity for the tracers, mostly occurring from about 2.0 ms onward. A significant part of the late-time velocities may be attributable to tracers from this set being swept up in what may be largely a flow of air and explosive products mixed with water. This is consistent with the upward flow of explosive products seen clearly in Figures 8 through 10 and the large shear forces that must also exist at the left surface of the barricade.

The trapezoidal shape of the barricade can be viewed as a composite structure (see Figure 6, looking from left to right) of a right triangle with its hypotenuse (the front surface) at the left, a 1.0-m-thick rectangle at the core, and a right triangle with its hypotenuse (the rear surface) at the right. Twenty tracers were evenly distributed, bottom to top, just inside the front "surface" of this inner 1.0-m-thick rectangle. The unweighted average overpressure versus time of these tracers is shown in Figure 17. The peak value of the overpressure of 324.6 MPa (47,080 psi) occurred at 1.78 ms. It is greater by 10.5 percent than the peak average value for the left surface of the barricade in Figure 15. This is primarily because this set of tracers is initially vertical and relatively deep within the water. The region of

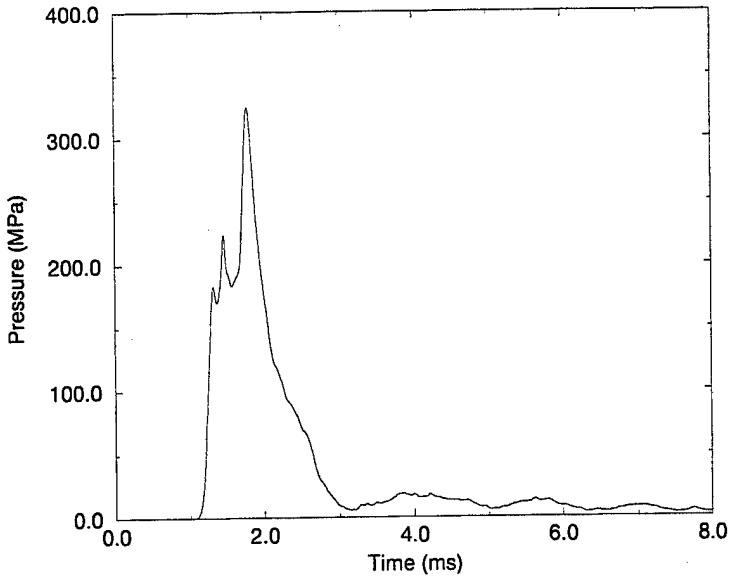

Figure 17. Average Overpressure Inside the Left Surface of the 1.0-m-Thick Core of the Water Barricade, Computation 970908.

the computational flow field in which those tracers were initially placed is not subject to as rapidly varying an interaction as that which occurs on the sloping front surface. The front surface not only has much greater shear forces but also has more rapidly occurring pressure relief waves. The average X-direction velocity versus time for the set of tracers along the front of the barricade core is shown in Figure 18. It shows a peak average velocity of 184.9 m/s at 1.79 ms and a late-time average velocity of 164.9 m/s at 8.0 ms, both of which are close to the bulk velocity of 173.4 m/s at 8.0 ms for the entire barricade.

Twenty more tracers were evenly distributed, bottom to top, at the center of the inner 1.0-m-thick rectangle in the barricade. The unweighted average overpressure versus time of these tracers is shown in Figure 19. The peak value of the overpressure of 305.7 MPa (44,340 psi) occurred at 1.97 ms. It is 5.8 percent less than the peak average overpressure at the front of the core. The average X-direction velocity versus time for this set of tracers along the vertical center of the barricade core is shown in Figure 20. It shows a peak average velocity of 163.8 m/s at 1.97 ms and a late-time average velocity of 171.3 m/s at 8.0 ms, both of which are close to the bulk velocity of 173.4 m/s at 8.0 ms for the entire barricade.

Moving farther to the right into the barricade, 20 more tracers were evenly distributed, bottom to top, just inside the back surface of the inner 1.0-m-thick rectangle in the barricade. The unweighted average overpressure versus time of these tracers is shown in Figure 21. The peak value of the overpressure of 255.5 MPa (37,060 psi) occurred at 2.16 ms. It is 16.4 percent less than the peak average overpressure at the center of the core, continuing the

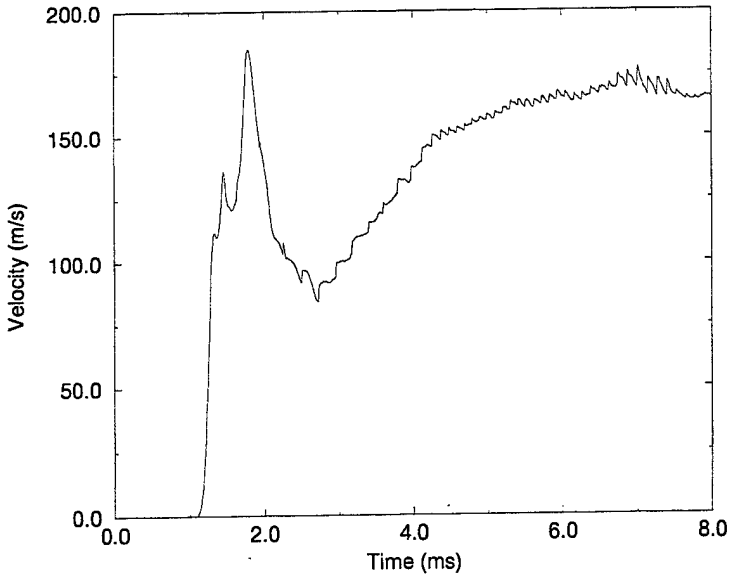

Figure 18. Average X-Direction Velocity Inside the Left Surface of the 1.0-m-Thick Core of the Water Barricade, Computation 970908.

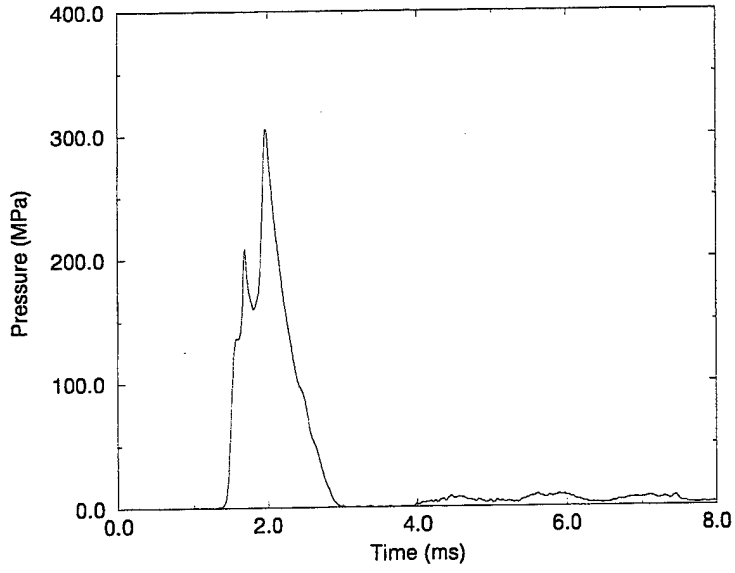

Figure 19. Average Overpressure at the Center of the 1.0-m-Thick Core of the Water Barricade, Computation 970908.

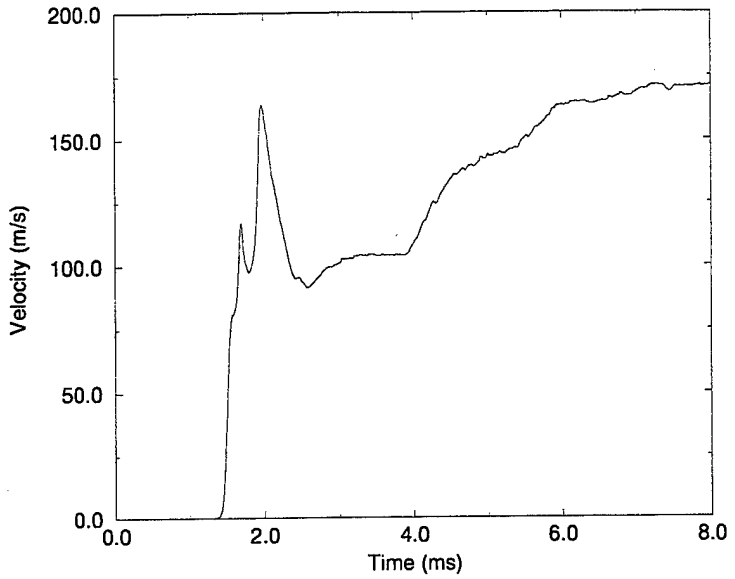

Figure 20. Average X-Direction Velocity Along the Vertical Center of the 1.0-m-Thick Core of the Water Barricade, Computation 970908.

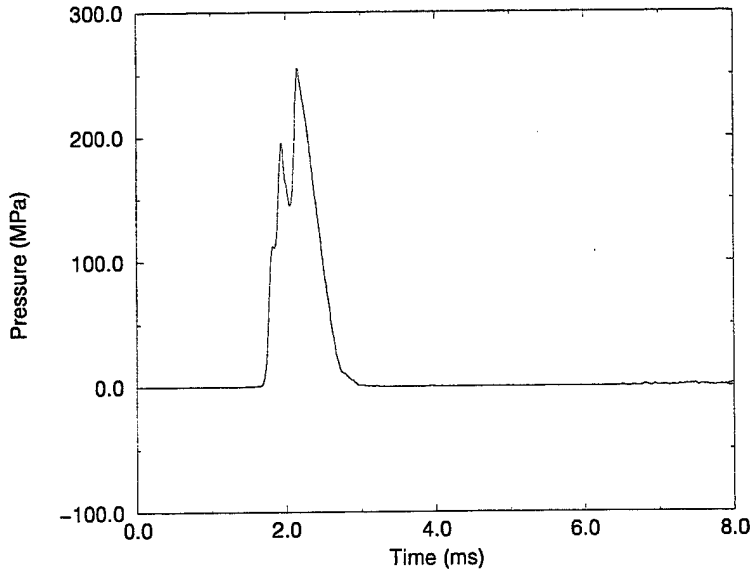

Figure 21. Average Overpressure Along the Back Surface of the 1.0-m-Thick Core of the Water Barricade, Computation 970908.

trend of decreasing interior pressures moving from front to back, as would be expected. The average X-direction velocity versus time for this set of tracers along the back surface of the barricade core is shown in Figure 22. It shows a peak average velocity of 146.7 m/s at 2.18 ms

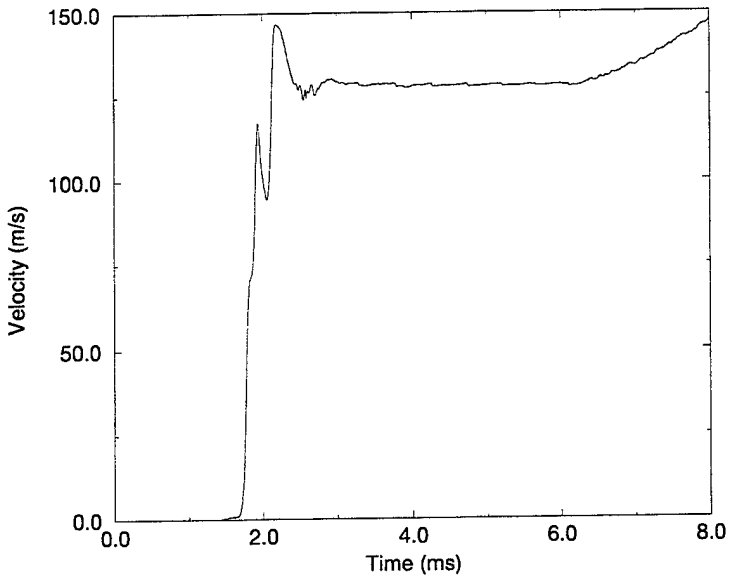

Figure 22. Average X-Direction Velocity Along the Back Surface of the 1.0-m-Thick Core of the Water Barricade, Computation 970908.

and a late-time average velocity of 147.2 m/s at 8.0 ms, both of which are low relative to the bulk velocity of 173.4 m/s at 8.0 ms for the entire barricade.

Another set of 20 tracers was placed just under the sloping back surface of the barricade. They were evenly distributed, bottom to top, in symmetric opposition to those placed under the sloping front surface. The unweighted average overpressure versus time of these tracers is shown in Figure 23. The curve is extremely noisy, with many sharp, brief peaks, the greatest of which is 45.23 MPa (6,560 psi) at 2.60 ms. This is indicative of spalling conditions at the rear surface of the water, with strong expansion waves moving back into the water to rapidly relieve pressure after the arrival of shocks and strong compression waves at the rear surface. It also may be caused by having at least some of the tracers moving out of cells of pure water and into mixed-material cells. The average X-direction velocity versus time for this set of tracers along the back surface of the barricade core is shown in Figure 24. It shows a peak average velocity of 258.1 m/s at 2.68 ms and a late-time average velocity of 235.8 m/s at 8.0 ms, which is 36.0 percent greater than the bulk velocity of 173.4 m/s at 8.0 ms for the entire barricade. Thus, Figures 23 and 24 are consistent in their indication of a spalling condition at the rear surface of the barricade but not at a particularly high velocity relative to that of the rest of the structure.

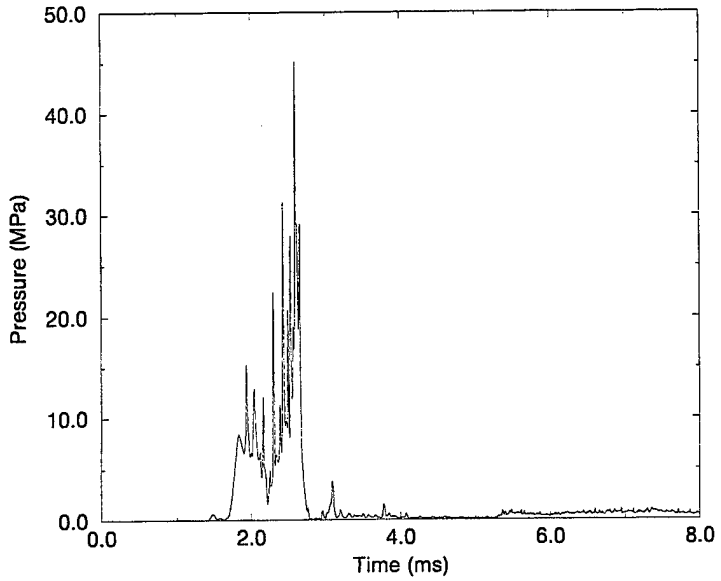

Figure 23. Average Overpressure Along the Sloping Rear Surface of the Water Barricade, Computation 970908.

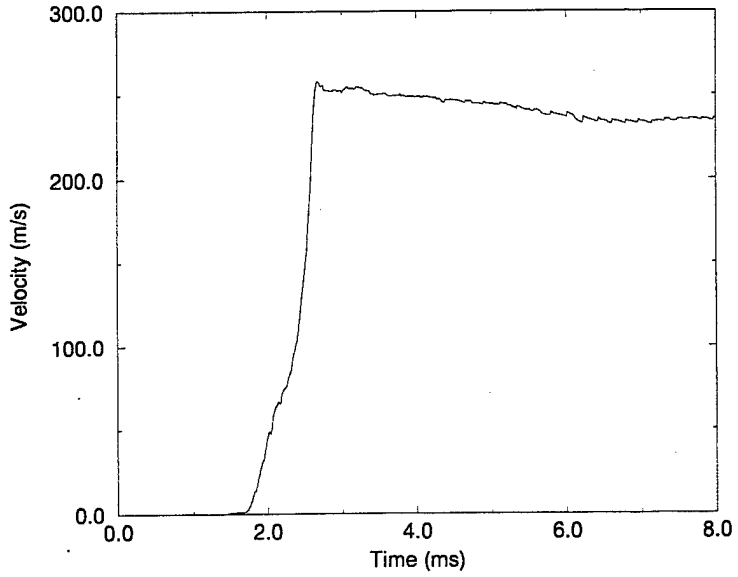

Figure 24. Average X-Direction Velocity Along the Sloping Rear Surface of the Water Barricade, Computation 970908.

Finally, a set of 30 evenly spaced tracers was placed along the left surface of the acceptor stack that faced the barricade and the donor stack beyond it. Specifically, they were placed in the first column of air-filled cells immediately in front of the iron block used to represent the acceptor stack. The unweighted average overpressure versus time for those tracers is shown in Figure 25. The average overpressure on the front surface of the acceptor stack reached a

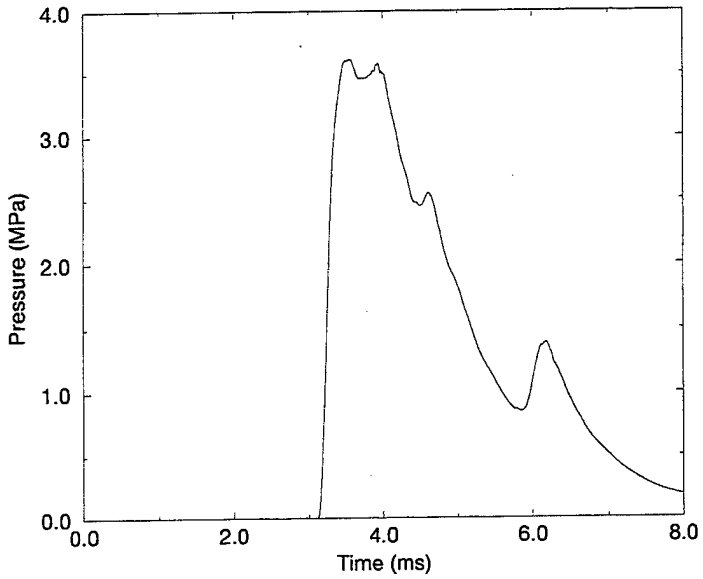

Figure 25. Average Overpressure Along the Front Surface of the Acceptor Stack, Computation 970908.

peak value of 3.61 MPa (524 psi) at 3.55 ms and had declined to 187 kPa (27.2 psi) by 8.0 ms. An analysis of Computation 970908 showed that this was caused only by the air blast. No explosive products of any consequence were computed to have reached the acceptor stack during this time.

The approximate bulk X-direction velocity versus time of the acceptor stack that was caused by the blast loading before the arrival of the water barricade is shown in Figure 26. This is shown primarily to document that the water barricade provides relatively good protection against direct blast loading for a simple high-order detonation event. Computation 970908 used a full-sized cross section for the acceptor stack and modeled it with iron, so the acceptor stack as modeled was much more massive than the actual stack. The velocity computed for Figure 26 used a corrected mass value, 118.61 kg/cm of depth, to produce the corrected velocity. This corrected velocity has a very minor intrinsic error in that the true movement of the stack during the loading time would reduce the loading but only by an extremely small amount in this case. The final velocity of the acceptor stack was relatively low at 1.58 m/s by 8.0 ms and essentially constant by that time. Differentiating that velocity with respect to time produces the acceleration versus time of the acceptor stack, which is

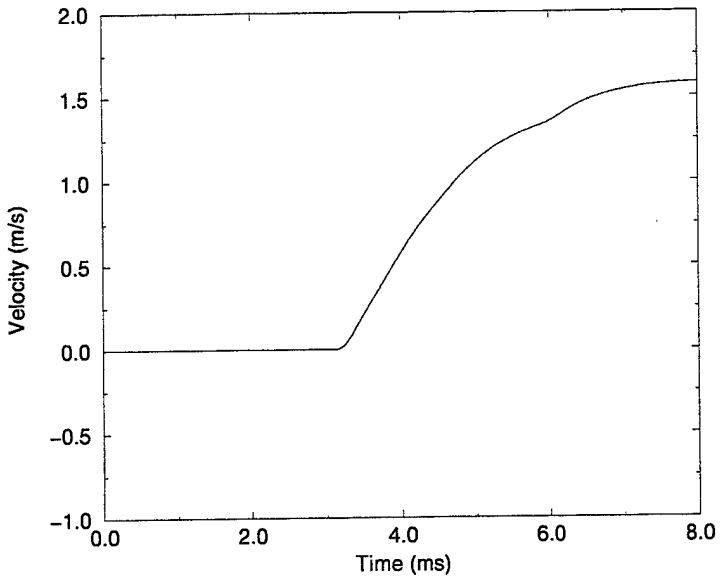

Figure 26. Acceptor Stack X-Direction Velocity Attributable to Blast Loading, Computation 970908.

shown in Figure 27. A peak acceleration of 79.5 G's is reached at 3.48 ms. It is highly unlikely that this in itself could be a threat to initiate the munitions in the stack.

An estimate can be made of the expected arrival time of the main body of the barricade at the acceptor stack front surface. By 8.0 ms, the barricade had moved 101.8 cm and was traveling in the X direction at a velocity of 173.4 m/s. The initial standoff of the acceptor stack from the barricade was 3.048 m. The time required to travel the remaining distance of 2.03 m at that velocity is 11.7 ms, so the estimated arrival time of the barricade at the acceptor front surface is 19.7 ms after initiation. This estimate does not include a correction for the distortion of the barricade during the loading event.

3.2. Barricade Translation and Acceptor Stack Loading and Response

As stated previously, Computation 971001 was set up to model the impact of the barricade against the acceptor stack. The barricade was reconstituted into its original mass and trapezoidal shape and assigned an initial X-direction velocity of 173.4 m/s, the final velocity from Computation 970908. The Y-direction (vertical) velocity from 970908, which was judged not to be of first-order importance, was set to zero for this computation. As stated previously, the acceptor stack was modeled in 971001 as being made of iron, having the correct height but having the width adjusted so that its mass per unit depth was correct at 118.61 kg/cm depth. Its relatively low, final X-direction velocity of 1.58 m/s at 8.0 ms

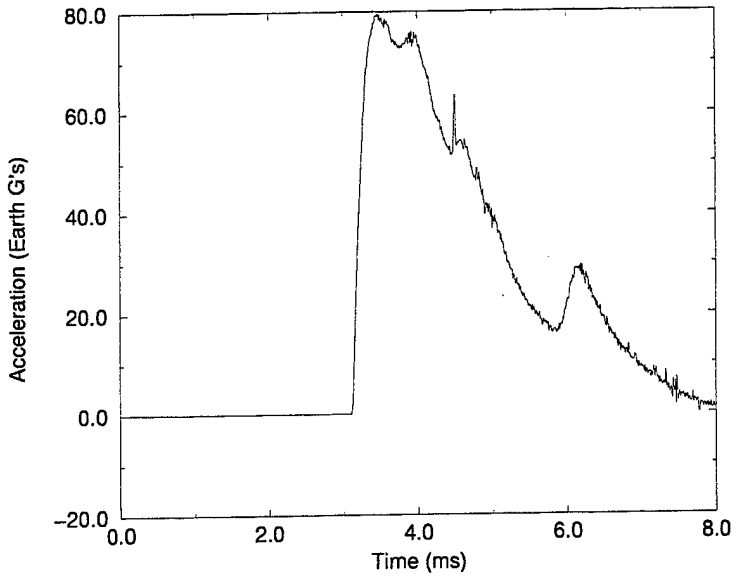

Figure 27. Acceptor Stack X-Direction Acceleration Due to Blast Loading, Computation 970908.

in Computation 970908 was ignored. The translating barricade was placed in the CTH computational flow field with its right-most bottom corner ready to impact the bottom-left surface of the acceptor stack. For convenience in Computation 971001, the time at the start of this computation was set to zero. Adding 19.7 ms to the time in this computation would give a reasonably good reference back to the time of the event, relative to the initiation of the donor stack. Figure 28 shows the computational flow field at the start of Computation 971001, with the rear surface of the translating water barricade ready to impact the acceptor stack. The air is shown in the yellow region, the borders of which also define the limits of the computational flow field. The water barricade is shown as the blue trapezoid and the acceptor stack as the black rectangle. Pressure contours, which are not of critical interest for this discussion, are shown as white-out lines to give a qualitative indication of the pressure fields in the grid. Figure 29 shows the flow field at 1.00 ms. The water is beginning to stagnate against the bottom of the acceptor stack surface. Compression waves have been transmitted into the acceptor stack and reflected into the barricade. Figure 30 shows the flow field at 2.00 ms. The stagnation of the water from the rear surface of the barricade is progressing up the front surface of the acceptor stack, and the reflected compression waves in the barricade have almost reached its front (i.e., left) surface. Figure 31 shows that by 5.00 ms, the front surface of the acceptor stack has been fully engaged by the water barricade, and a small amount of water is jetting upward above the top of the acceptor stack. The computation ran until it failed at 7.81 ms, when the degree of scattering and mixing of water, air, and possibly iron seems to have exceeded the capacity of the modeling of this

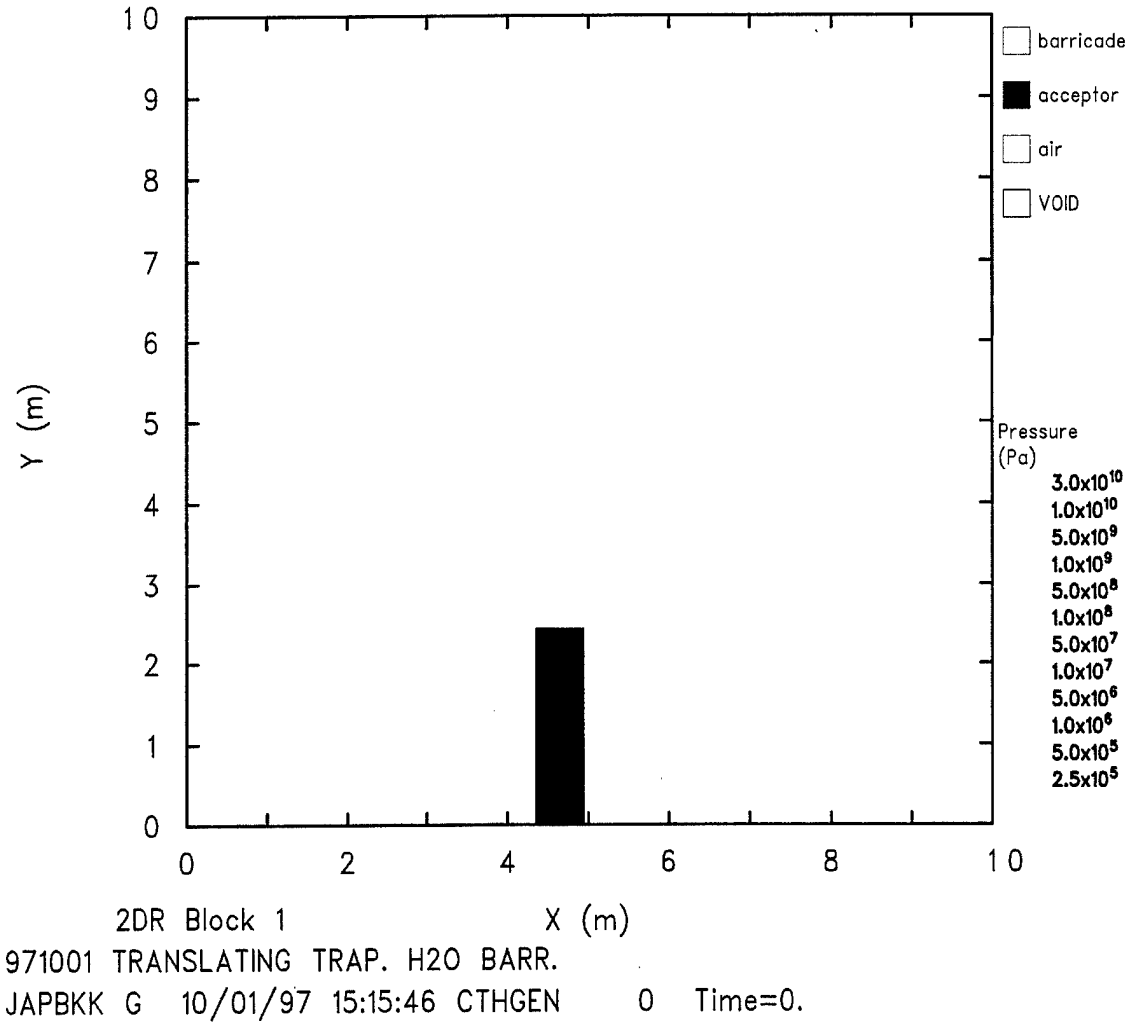

Figure 28. Flow Field at Time = 0.00 for Computation 971001.

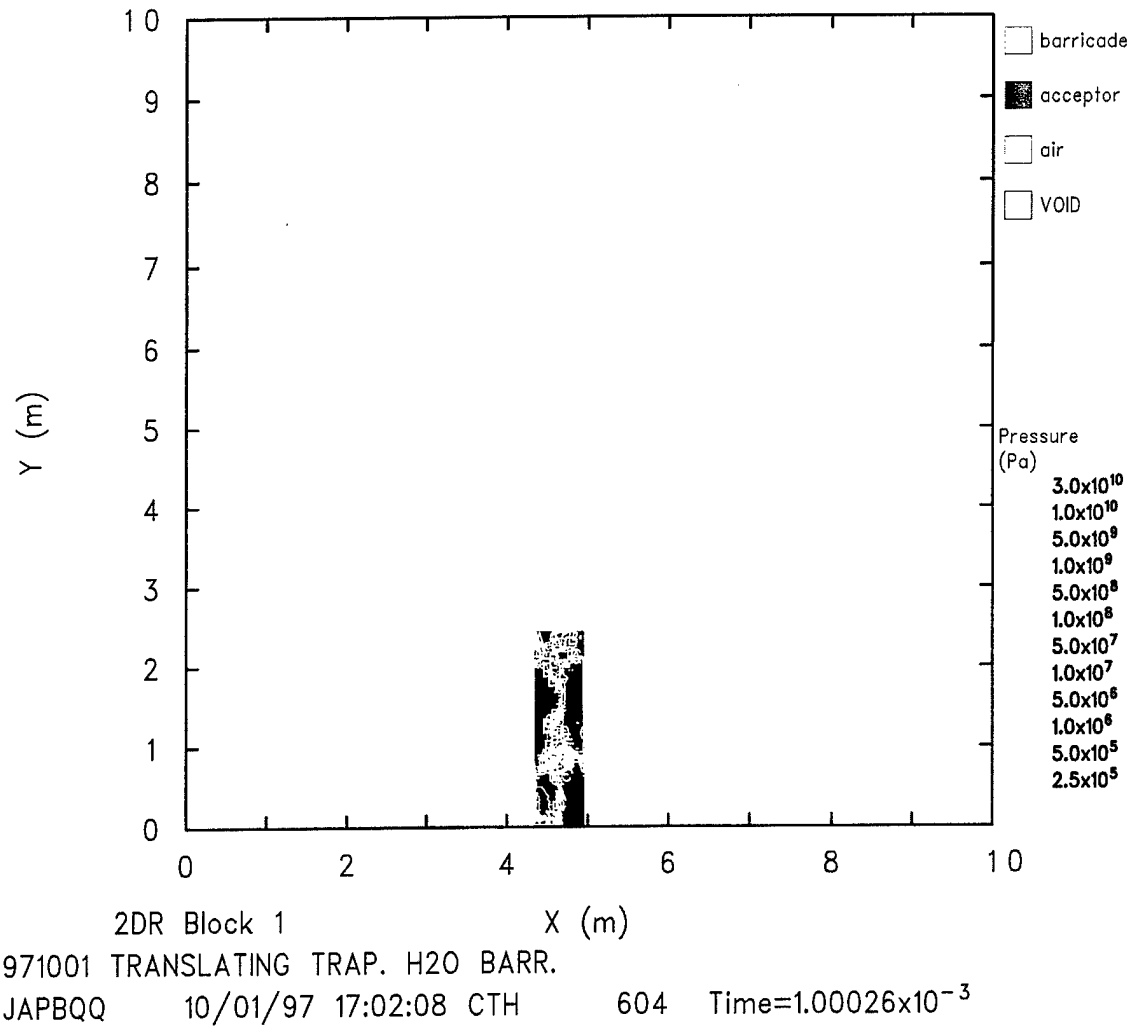

Figure 29. Flow Field at Time = 1.00 ms for Computation 971001.

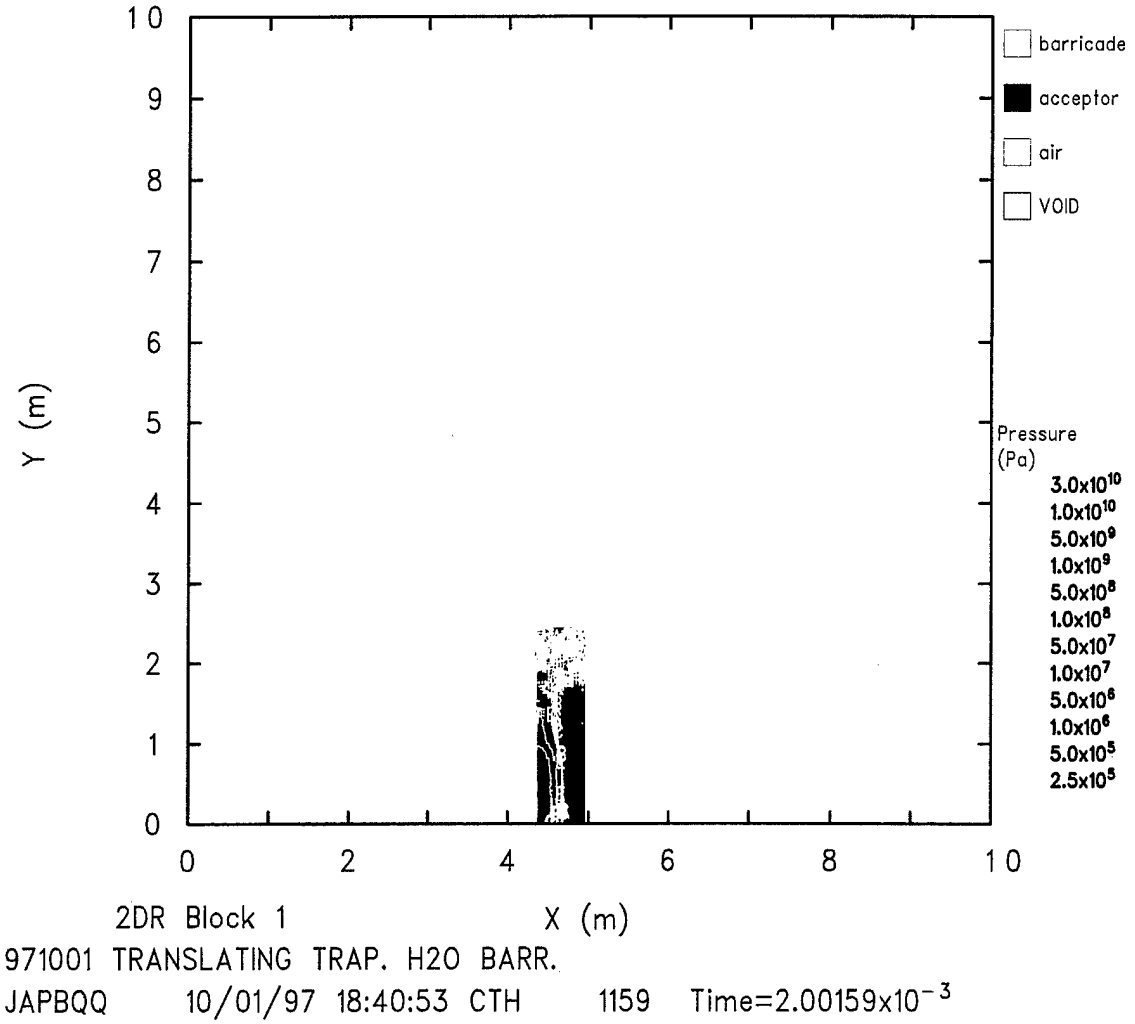

Figure 30. Flow Field at Time = 2.00 ms for Computation 971001.

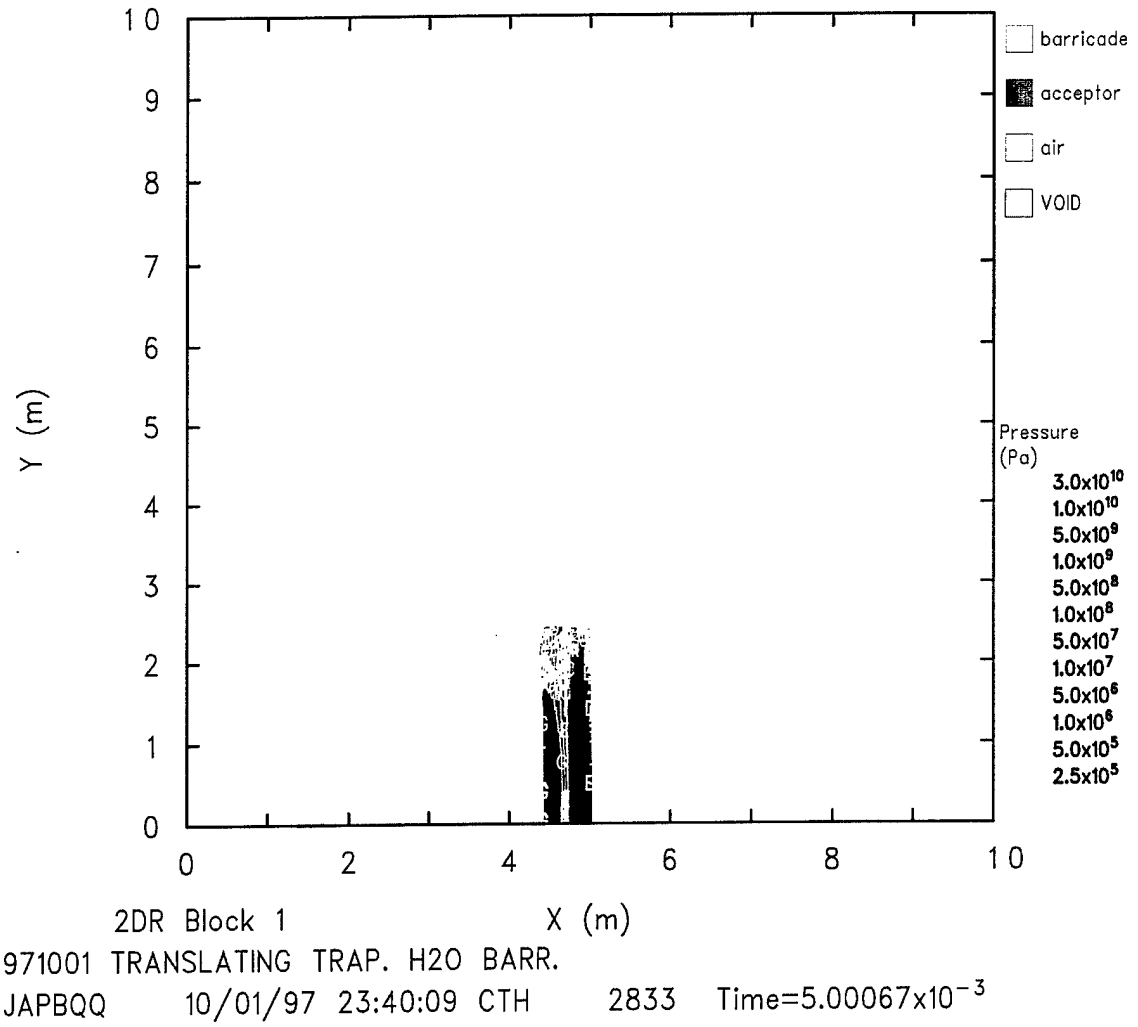

Figure 31. Flow Field at Time = 5.00 ms for Computation 971001.

particular problem within CTH to produce thermodynamically consistent results. That flow field is shown in Figure 32. Because the acceptor stack had reached a steady-state velocity by that time, there was no attempt to stabilize the computation and continue progressing in time.

Figure 33 shows the velocity versus time for the barricade as it interacts with the acceptor stack. As momentum is transferred to the acceptor stack, the velocity of the barricade decreases, reaching a nearly steady value of 92.5 m/s by 7.80 ms, a decrease of 46.7 percent from its initial value of 173.4 m/s. Figure 34 shows the acceleration versus time of the water barricade as it interacts with the acceptor stack. Negative values indicate deceleration, with a peak deceleration of 2,127 G's for the barricade occurring at 3.47 ms.

Figure 35 shows the velocity versus time for the acceptor stack in response to the impact and momentum transfer from the barricade. At the ending time of the computation at 7.80 ms, the acceptor stack has reached a nearly steady velocity of 40.0 m/s, or approximately 41.6 m/s if the 1.6 m/s ending velocity from Computation 970908 is added under a linear superposition assumption. Figure 36 shows the acceleration versus time of the acceptor stack. It has a relatively small peak acceleration of 1,053 G's at 3.62 ms. Finally, Figure 37 shows the distance that the acceptor stack is moved during the time simulated in Computation 971001. The displacement of the acceptor stack is 17.0 cm at the ending time of 7.80 ms.

4. CONCLUSION

The computations discussed herein provide an estimate of the blast loading from a simplified, uncased explosive charge representing a nominal munitions stack of 4,000 kg of Comp-B undergoing a complete, high-order detonation. No munitions casing (and their resulting fragments) or packing materials were included. Because the computation was performed in a 2-D Cartesian coordinates system, this provided a worst case estimate of the blast loading because of the elimination of 3-D divergence effects. In an actual detonation event, a munitions stack would not behave as the simple, monolithic charge modeled here. There would be a series of detonation events for the individual munitions, spreading outward from the first item that detonated in a pattern based on combinations of fragment impacts and sympathetic detonations.

The loading on and response of a water barricade having a trapezoidal cross section were computed. The water barricade was effective in deflecting most of the blast and nearly all of the explosive products upward and away from the acceptor stack. By 8.0 ms, the water barricade had accelerated to a nearly steady bulk velocity of 173.4 m/s toward the acceptor stack and had undergone significant distortion. That distortion indicated that large shearing forces occurred on and within the barricade but that this simplified shape maintained enough integrity during the loading event to be effective. An actual water barricade would have voids, shells and/or bladders, and various reinforcements and attachments that would greatly

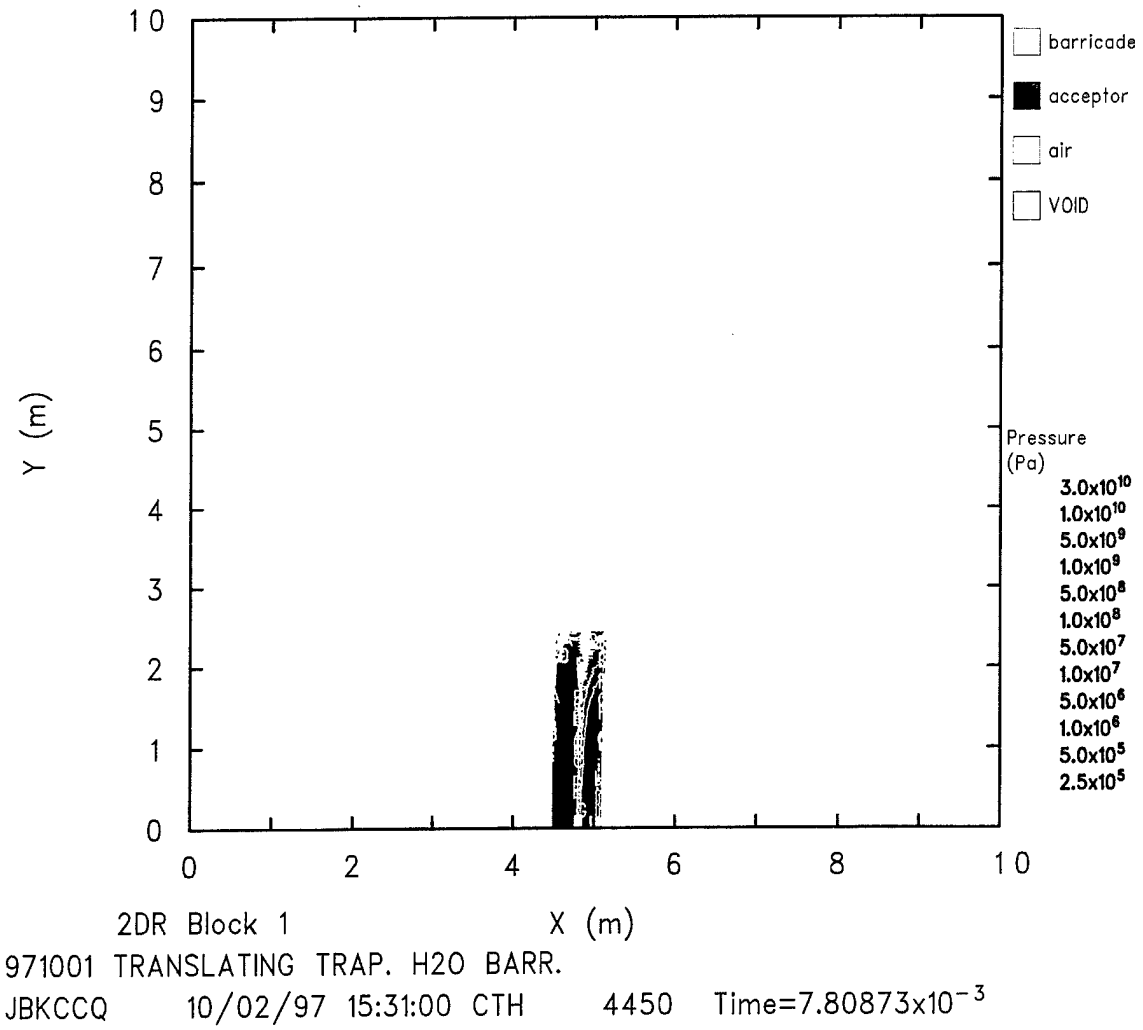

Figure 32. Flow Field at Time = 7.81 ms for Computation 971001.

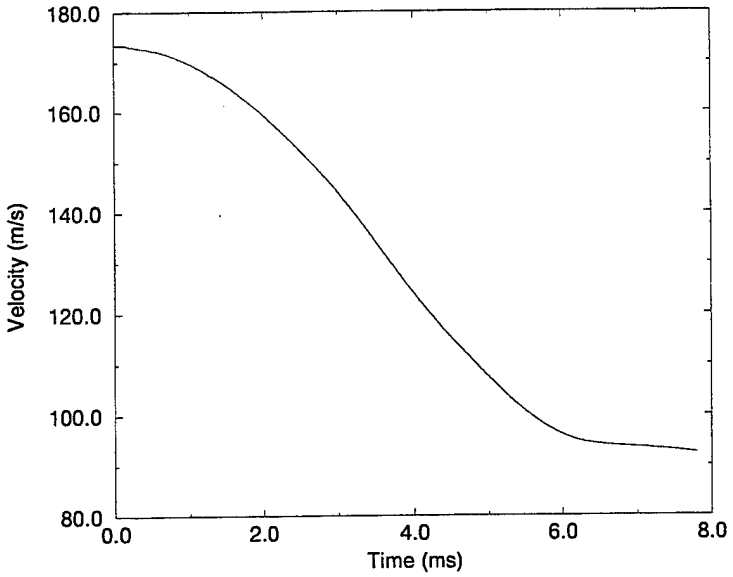

Figure 33. Barricade X-Direction Velocity for Computation 971001.

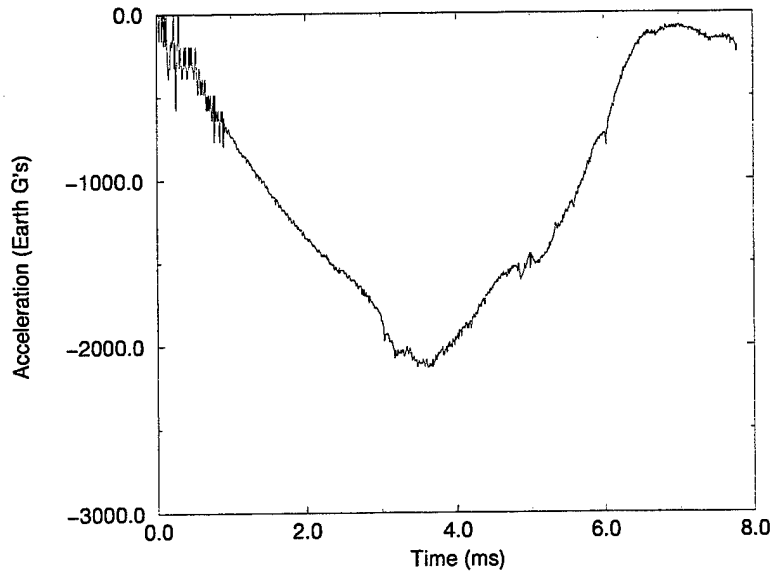

Figure 34. Barricade X-Direction Acceleration for Computation 971001.

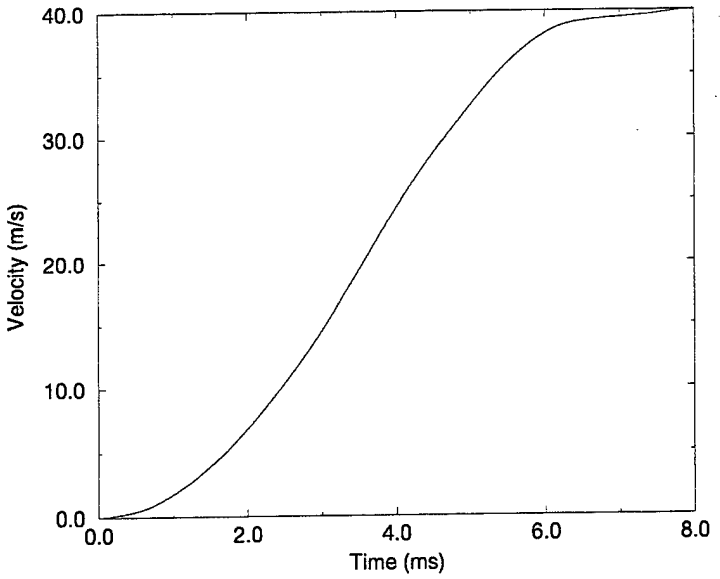

Figure 35. Acceptor Stack X-Direction Velocity for Computation 971001.

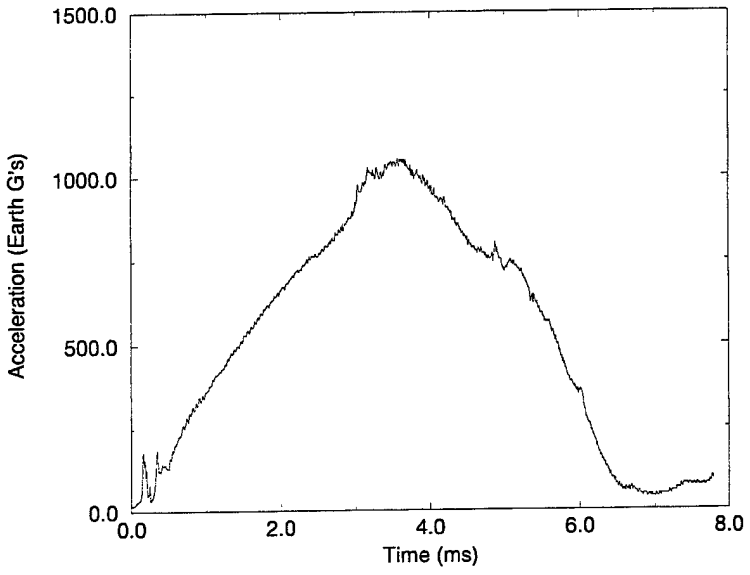

Figure 36. Acceptor Stack X-Direction Acceleration for Computation 971001.

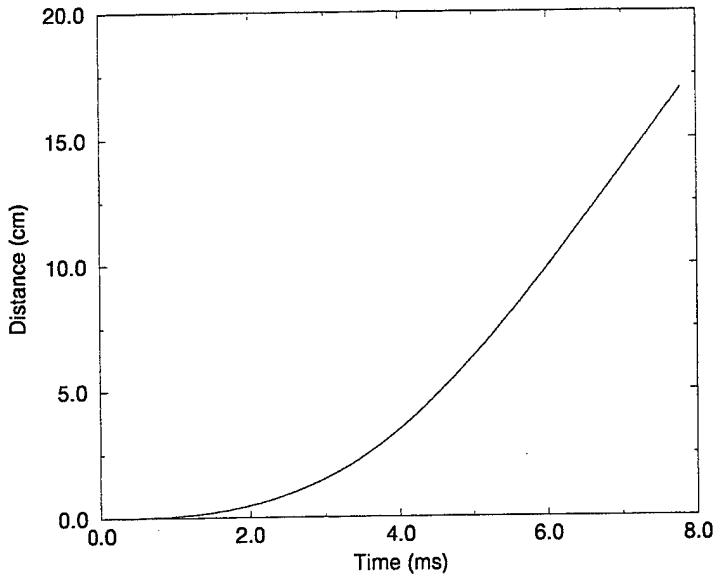

Figure 37. Acceptor Stack X-Direction Distance Moved for Computation 971001.

affect its strength and disintegration under blast and fragment loading. The amount of water required for this assumed shape may be impractical in field operations in which water supplies are not plentiful. No analysis of how practical such a water barricade would be to erect and maintain was performed.

The blast loading on the acceptor stack in this assumed configuration was minimal, as was the resulting acceleration, or G-loading, of the acceptor stack. The impact of the mathematically reconstituted water barricade at the 173.4-m/s velocity produced only moderate loading on and acceleration of the acceptor stack. No threat of causing a sympathetic detonation of the acceptor stack was indicated. The same comments concerning the donor stack also apply to the acceptor stack. An actual donor munitions stack would not respond as does a monolithic block such as the one modeled here. Even a relatively modest blast load would disrupt and scatter the munitions, with random events causing a possibly significant distribution of velocities and impacts for individual munitions.

Additional computational studies in this part of the overall effort will be performed to evaluate other barricade shapes (e.g., rectangles of different thicknesses) and materials (e.g., sand) to determine their effectiveness. Computational studies of the impact of various barricade materials and their equivalents on simulated munitions will also be performed.

INTENTIONALLY LEFT BLANK

REFERENCES

1. J.M. McGlaun, S.L. Thompson, L.N. Kmetck, and M.G. Elrick, "A Brief Description of the Three-Dimensional Shock Wave Physics Code CTH," SAND 89-0607, Sandia National Laboratories, Albuquerque, NM, July 1990.

2. R.L. Bell, M.R. Baer, R.M. Brannon, M.G. Elrick, A.V. Farnsworth, E.S. Hertel, S.V. Petney, S.A. Silling, and P.A. Taylor, "CTHGEN User's Manual and Input Instructions, Version 3.00," CTH Development Project, Sandia National Laboratories, Albuquerque, NM, 18 July 1996.

3. R.L. Bell, M.R. Baer, R.M. Brannon, M.G. Elrick, A.V. Farnsworth, E.S. Hertel, S.V. Petney, S.A. Silling, and P.A. Taylor, "CTH User's Manual and Input Instructions, Version 3.00," CTH Development Project, Sandia National Laboratories, Albuquerque, NM, 18 July 1996.

4. J. Starkenberg, K.J. Benjamin, R.B. Frey, "Predicting Fragmentation Propagation Probabilities for Ammunition Stacks," ARL-TR-949, U.S. Army Research Laboratory, APG, MD, January 1996.

5. "Technical Manual. Army Ammunition Data Sheets. Artillery Ammunition. Guns, Howitzers, Mortars, Recoilless Rifles, Grenade Launchers, and Artillery Fuzes." TM-43-0001-28, Headquarters, Department of the Army, April 1977.

6. G.I. Kerley and T.L. Christian Frear, "Composition B-3 Detonation Products," SAND93-2131, Sandia National Laboratories, Albuquerque, NM, 1993.

7. G.I. Kerley, "CTH Reference Manual: The Equation of State Package," SAND91-0344, Sandia National Laboratories, Albuquerque, NM, 24 May 1991.

8. B.M. Dobratz and P.C. Crawford, "LLNL Explosives Handbook, Properties of Chemical Explosives and Explosive Simulants," UCRL-52997, Change 2, Lawrence Livermore National Laboratory, Livermore, CA, 31 January 1985.

9. Federal-Fabrics-Fibers, Inc., "Rapid Ammunition Barricade Technology Development," Small Business Innovative Research Contract DAAE30-97-C-1023, 10 March 1997.

10. F.H. Ree, "Equation of State for Water," UCRL-52190, Lawrence Livermore National Laboratory, Livermore, CA, December 1976.

11. G.I. Kerley, "Multiphase Equation of State for Iron," SAND93-0227, Sandia National Laboratories, Albuquerque, NM, 1993.

12. H.C. Graboske, UCID-16901, data for dry air, December 1981, modified March 1992.

INTENTIONALLY LEFT BLANK

NO. OF COPIES ORGANIZATION

2 ADMINISTRATOR
DEFENSE TECH INFO CENTER
ATTN DTIC DDA
8725 JOHN J KINGMAN RD STE 0944
FT BELVOIR VA 22060-6218

1 DIRECTOR
US ARMY RESEARCH LAB
ATTN AMSRL CS AL TA REC MGMT
2800 POWDER MILL RD
ADELPHI MD 20783-1197

1 DIRECTOR
US ARMY RESEARCH LAB
ATTN AMSRL CI LL TECH LIB
2800 POWDER MILL RD
ADELPHI MD 207830-1197

1 DIRECTOR
US ARMY RESEARCH LAB
ATTN AMSRL CS AL TP TECH PUB BR
2800 POWDER MILL RD
ADELPHI MD 20783-1197

1 DIR OF DEFENSE RESEARCH
AND ENGINEERING
ATTN DD/TWP
WASHINGTON DC 20301

1 COMMANDER
FIELD COMMAND DSWA
ATTN FCTTS E MARTINEZ
KIRTLAND AFB NM 87115

1 DIRECTOR
ADVANCED RSCH PROJECTS AGENCY
ATTN TECHNICAL LIBRARY
3701 NORTH FAIRFAX DRIVE
ARLINGTON VA 22203-1714

1 COMMANDER
US ARMY ARDEC
ATTN SMCAR FSM W/BARBER
BLDG94
PICATINNY ARSENAL NJ 07806-5000

NO. OF COPIES ORGANIZATION

1 COMMANDER
US ARMY ENGINEER DIVISION
ATTN HNDED FD
PO BOX 1500
HUNTSVILLE AL 35807

1 COMMANDER
US ARMY CORPS OF ENGINEERS
FT WORTH DISTRICT
ATTN CESWF PM J
PO BOX 17300
FORT WORTH TEXAS 76102-0300

1 COMMANDER
US ARMY RESEARCH OFFICE
ATTN SLCRO D
PO BOX 12211
RESEARCH TRIANGLE PARK NC
27709-2211

1 COMMANDER
DAVID TAYLOR RESEARCH CENTER
ATTN CODE 522 TECH INFO CTR
BETHESDA MD 20084-5000

1 OFFICER IN CHARGE (CODE L31)
CIVIL ENGINEERING LABORATORY
NAVAL CONST BATTALION CENTER
ATTN TECHNICAL LIBRARY
PORT HUENEME CA 93041

1 COMMANDER (CODE 533)
NAVAL WEAPONS CENTER
ATTN TECHNICAL LIBRARY
CHINA LAKE CA 93555-6001

1 COMMANDER
DAHLGREN DIVISION
NAVAL SURFACE WARFARE CENTER
ATTN CODE E23 LIBRARY
DAHLGREN VA 22448-5000

1 COMMANDER
NAVAL RESEARCH LABORATORY
ATTN CODE 2027 TECH LIBRARY
WASHINGTON DC 20375

NO. OF COPIES ORGANIZATION

1 COMMANDER
NAVAL WEAPONS EVAL FAC
ATTN DOCUMENT CONTROL
KIRTLAND AFB NM 87117

2 AIR FORCE ARMAMENT LAB
ATTN AFATL/DOIL
AFATL/DLYV
EGLIN AFB FL 32542-5000

1 DIRECTOR
LAWRENCE LIVERMORE NATL LAB
ATTN TECH INFO DEPT L 3
PO BOX 808
LIVERMORE CA 94550

1 NAIC/DXLA
ATTN TECHNICAL LIBRARY
4180 WATSON WAY
WRIGHT PATTERSON AFB OH
45433-5648

1 KAMAN SCIENCES CORPORATION
ATTN LIBRARY
PO BOX 7463
COLORADO SPRINGS CO 80933-7463

1 DIRECTOR
SANDIA NATL LABORATORIES
ATTN DOC CONTROL 3141
PO BOX 5800
ALBUQUERQUE NM 87185-5800

1 LOS ALAMOS NATL LABORATORY
REPORT COLLECTION CID 14 MS P364
PO BOX 1663
LOS ALAMOS NM 87545

1 REPORT COLLECTION CIC 14
MS P364
LOS ALAMOS NATL LABORATORY
LOS ALAMOS NM 87545

1 REPORT COLLECTION
RESEARCH LIBRARY MS P362
PO BOX 7113
LOS ALAMOS NM 87544-7113

NO. OF COPIES ORGANIZATION

1 DIRECTOR
SANDIA NATIONAL LABORATORIES
LIVERMORE LABORATORY
ATTN DOC CONTROL FOR TECH LIB
PO BOX 969
LIVERMORE CA 94550

1 DIRECTOR
NASA LANGLEY RESEARCH CENTER
ATTN TECHNICAL LIBRARY
HAMPTON VA 23665

1 SUNBURST RECOVERY INC
ATTN DR C YOUNG
PO BOX 2129
STEAMBOAT SPRINGS CO 80477

2 SRI INTERNATIONAL
ATTN DR J GRAN
DR B HOLMES
333 RAVENWOOD AVENUE
MENLO PARK CA 94025

2 DENVER RESEARCH INSTITUTE
ATTN J WISOTSKI
TECHNICAL LIBRARY
PO BOX 10758
DENVER CO 80210

3 SOUTHWEST RESEARCH INST
ATTN DR C ANDERSON
S MULLIN
A B WENZEL
PO DRAWER 28255
SAN ANTONIO TX 78228-0255

1 CECOM
SP & TERRESTRIAL COM DIV
ATTN AMSEL RD ST MC M
H SOICHER
FT MONMOUTH NJ 07703-5203

1 PRIN DPTY FOR TECH GY HDQ
US ARMY MATL CMND
ATTN AMCDCG T M FISETTE
5001 EISENHOWER AVE
ALEXANDRIA VA 22333-0001

NO. OF COPIES ORGANIZATION

1 PRIN DPTY FOR ACQTN HDQ
US ARMY MATL CMND
ATTN AMCDCG A D ADAMS
5001 EISENHOWER AVE
ALEXANDRIA VA 22333-0001

1 DPTY CG FOR RDE HDQ
US ARMY MATL CMND
ATTN AMCRD BG BEAUCHAMP
5001 EISENHOWER AVE
ALEXANDRIA VA 22333-0001

1 DPTY ASST SCY FOR RSRCH & TECH
SARD-TT F MILTON RM 3EA79
THE PENTAGON
WASHINGTON DC 20310-0103

1 ODCSOPS
D SCHMIDT
WASHINGTON DC 20310-1001

1 OSD
OUSD(A&T)/ODDDR&E(R) J LUPO
THE PENTAGON
WASHINGTON DC 20301-7100

1 ARL ELECTROMAG GROUP
CAMPUS MAIL CODE F0250 A TUCKER
UNIVERSITY OF TEXAS
AUSTIN TX 78712

1 DUSD SPACE
1E765 J G MCNEFF
3900 DEFENSE PENTAGON
WASHINGTON DC 20301-3900

1 USAASA
MOAS-AI W PARRON
9325 GUNSTON RD STE N319
FT BELVOIR VA 22060-5582

1 CECOM
PM GPS COL S YOUNG
FT MONMOUTH NJ 07703

1 GPS JOINT PROG OFC DIR
COL J CLAY
2435 VELA WAY STE 1613
LOS ANGELES AFB CA 90245-5500

NO. OF COPIES ORGANIZATION

1 ELECTRONIC SYSTEMS DIV DIR
CECOM RDEC
J NIEMELA
FT MONMOUTH NJ 07703

3 DARPA
L STOTTS
J PENNELLA
B KASPAR
3701 N FAIRFAX DR
ARLINGTON VA 22203-1714

1 SPECIAL ASST TO THE WING CDR
50SW/CCX CAPT P H BERNSTEIN
300 O'MALLEY AVE STE 20
FALCON AFB CO 80912-3020

1 USAF SMC/CED
DMA/JPO M ISON
2435 VELA WAY STE 1613
LOS ANGELES AFB CA 90245-5500

1 UNIV OF MARYLAND
ATTN DR R DICK
RM 2168 ENGRG CLASSROOM BLDG
COLLEGE PARK MD 20742-5121

1 US NAVAL ACADEMY
ATTN TECH LIBRARY
572 HOLLOWAY ROAD
ANNAPOLIS MD 21402-5002

1 OLIN ORDNANCE
ATTN TECH LIB J KIBIGER
PRODUCT MATERIAL CONTROL
10101 9TH ST N
ST PETERSBURG FL 33716

1 COMMANDER
INDIAN HEAD DIV/NAVAL SURFACE WARFARE CENTER
ATTN CODE 950T M SWISDAK
101 STRAUSS AVENUE
INDIAN HEAD MD 20640-5035

1 COMMANDING OFFICER
NFESC
ATTN JIM TANCRETO ESC62
1100 23RD AVE BLDG 1100
PORT HUENEME CA 93043-4370

NO. OF
COPIES ORGANIZATION

1 CHAIRMAN
DOD EXPLOSIVES SAFETY BOARD
ATTN DR J WARD
HOFFMAN BLDG I ROOM 856C
2461 EISENHOWER AVENUE
ALEXANDRIA VA 22331-0600

1 DEFENSE AMMOLOG ACTIVITY
ATTN AMSTA AR AL
D SCARBOROUGH
PICATINNY ARSENAL NJ 07806-5000

1 US ARMY SOLDIER SYSTEMS CMD
ATTN SSCNS WSO DAVE LEMOINE
KANSAS STREET
NATICK MA 01760-5018

3 USAE WATERWAYS EXP STN
ATTN CEWES SD R P KINNEBREW
DR B CARNES
CEWES TL TECH LIB
3909 HALLS FERRY ROAD
VICKSBURG MS 39180-6199

1 US MILITARY ACADEMY
MATH SCI CTR OF EXCELLENCE
DEPT OF MATHEMATICAL SCI
MDN A MAJ DON ENGEN
THAYER HALL
WEST POINT NY 10996-1786

1 DIR SNL
ES HERTEL JR MS 0819
PO BOX 5800
ALBUQUERQUE NM 87185-0307

1 KERLEY PUB SUC
G I KERLEY
PO BOX 13835
ALBUQUERQUE NM 87192-3835

ABERDEEN PROVING GROUND

2 DIRECTOR
US ARMY RESEARCH LAB
ATTN AMSRL CI LP (TECH LIB)
BLDG 305 APG AA

NO. OF
COPIES ORGANIZATION

1 COMMANDER
US ARMY TECOM
ATTN AMSTE TE F (L TELETSKI)
RYAN BLDG APG

1 COMMANDER
US ARMY TEST CENTER
ATTN STEC LI
APG

28 DIRECTOR
US ARMY RESEARCH LAB
ATTN AMSRL WM MA W CHIN
T MULKERN C PERGANTIS
AMSRL WM PB B GUIDOS
H EDGE P PLOSTINS
P WEINACHT
AMSRL WM T W MORRISON
AMSRL WM TB V BOYLE
P BAKER T DORSEY
R FREY W HILLSTROM
W LAWRENCE R LOTTERO (5 CYS)
E MCDOUGAL J STARKENBERG
J WATSON
AMSRL WM TC K KIMSEY
D SCHEFFLER S SCHRAML
AMSRL WM TD P KINGMAN
M RAFTENBERG S SCHOENFELD

REPORT DOCUMENTATION PAGE

Form Approved OMB No. 0704-0188

1. AGENCY USE ONLY *(Leave blank)*	2. REPORT DATE	3. REPORT TYPE AND DATES COVERED
	March 1998	Final

4. TITLE AND SUBTITLE

Responses of a Water Barricade and an Acceptor Stack to the Detonation of a Donor Munitions Stack

5. FUNDING NUMBERS

PR: 1L162618AH80
NDE203

6. AUTHOR(S)

Lottero, R.E. (ARL)

7. PERFORMING ORGANIZATION NAME(S) AND ADDRESS(ES)

U.S. Army Research Laboratory
Weapons & Materials Research Directorate
Aberdeen Proving Ground, MD 21010-5066

8. PERFORMING ORGANIZATION REPORT NUMBER

9. SPONSORING/MONITORING AGENCY NAME(S) AND ADDRESS(ES)

U.S. Army Research Laboratory
Weapons & Materials Research Directorate
Aberdeen Proving Ground, MD 21010-5066

10. SPONSORING/MONITORING AGENCY REPORT NUMBER

ARL-TR-1600

11. SUPPLEMENTARY NOTES

12a. DISTRIBUTION/AVAILABILITY STATEMENT

Approved for public release; distribution is unlimited.

12b. DISTRIBUTION CODE

13. ABSTRACT *(Maximum 200 words)*

This report documents the numerical modeling of the detonation of a simplified munitions stack, referred to as the "donor" stack, in a temporary storage area and the subsequent effects on the immediate surroundings of the stack. A plausible configuration of a donor munitions stack, a water barricade, and an "acceptor" munitions stack is modeled in a two-dimensional (2-D) Cartesian hydrocode computation using the CTH hydrodynamics computer code. The donor stack is modeled as an uncased condensed high-explosive charge with a rectangular cross section. The water barricade has a trapezoidal cross section, and the acceptor stack is a solid rectangle. The loading on and pressures within the barricade are computed, as is the whole-body motion of the barricade. A separate computation was then run with the water barricade, reconstituted into its original shape and translating at the late-time velocity from the first computation, interacting with the acceptor stack. These computations were performed as part of a U.S. Army Research Laboratory (ARL) study entitled "Munitions Survivability Technology," sponsored by the U.S. Army Defense Ammunition Logistics (Ammolog) Activity.

14. SUBJECT TERMS

detonation
munitions survivability
munitions

15. NUMBER OF PAGES

55

16. PRICE CODE

17. SECURITY CLASSIFICATION OF REPORT	18. SECURITY CLASSIFICATION OF THIS PAGE	19. SECURITY CLASSIFICATION OF ABSTRACT	20. LIMITATION OF ABSTRACT
Unclassified	Unclassified	Unclassified	